Advancements and Challenges in Ciguatoxin Detection: Developing a High-Resolution Mass Spectrometric Method for the Identification of P-CTX-3B

A Thesis Submitted to the Committee on Graduate Studies in Partial Fulfillment of the Requirements for the Degree of Master of Science in the Faculty of Arts and Science

TRENT UNIVERSITY

Peterborough, ON, Canada

Environmental and Life Sciences M.Sc. Graduate Program

May 2024

Abstract

Advancements and Challenges in Ciguatoxin Detection: Developing a High- Resolution Mass Spectrometric method for the identification of P-CTX-3B
Natasha Prytulka

The detection of ciguatoxins (CTXs) in biological samples is challenging due to their low concentrations, the presence of various congeners, and the absence of standardized methods. This study uses high resolution mass spectrometry (HRMS) with P-CTX-3B as a reference standard. The protonated molecules ($[M+H]^+$) were most prevalent, especially when acetonitrile/water was utilized, providing enhanced sensitivity. Optimized collision energies of 15 eV for protonated molecules and flow rates of 10 µl/min enhance sensitivity and peak intensities, respectively. Acetonitrile/water (ACN/H_2O) is recommended as the primary solvent for HRMS method, an aspect underexplored in existing literature. The detection of CTX-3B in fish tissue samples proved to be challenging, caused by variations in ion peak intensities and matrix effects, requiring a deeper exploration of the impact of complex matrices on CTX detection. The study emphasizes the need for a reliable internal standard to mitigate these effects and highlights the ongoing challenge of developing a rapid, simple, and sensitive detection method. The study's specific focus on the P-CTX-3B analogue significantly contributes to methodology development for this congener, serving as a foundational step in understanding and detecting CTX. Despite notable progress, the study acknowledges the absence of an ideal assay, outlining key challenges for future research on ciguatera analysis. It underscores the continuous necessity for method reevaluation, testing, and the broader goal of establishing a more clarified and rugged method for the identification of CTX in fish.

Acknowledgements

I would like to acknowledge and express my gratitude to several individuals who have played pivotal roles in the successful completion of this thesis. First, I extend my sincere thanks to Dr. Holger Hintelmann, Dr. Naomi Stock, and Dr. Chris Metcalfe for not only providing me with this incredible opportunity but also for their guidance and invaluable assistance throughout my thesis. I am grateful to Dr. Mirelle and her team for supplying the standard for this project. I would also like to thank Linda Cardwell for her generosity and support towards me and fellow graduate students. Special thanks to Nikhil Pai Ganesh for being an unwavering pillar of support, offering both professional guidance and care as I navigated through my master's program. I extend my appreciation to Beatriz Bento, Una Jermilova, and the other lab mates for their kindness and motivation, which have been invaluable throughout this academic endeavor. To my parents, Victoria and Richard Mark Prytulka, whose enduring support and pride in my achievements have been a constant source of inspiration, I extend my thanks. To Latha and Ganesh Pai, for providing their support and thoughtfulness throughout the program. Lastly, I want to thank my extended family and friends for providing their unwavering encouragement by which I am truly grateful.

Table of Contents

List of Figures

fish sample) Blue: $[M+H-H_2O]^+$ Orange: $[M+H]^+$ Grey: $[M+NH4]^+$ Yellow: [M+Na]+. Figure A2: Concentration of fish sample spiked with 10, 20, 50, and 100 ppb of P-CTX3C standard after sample preparation and SPE versus peak intensity. Calibration solution 2 (prepared on a separate day from the spiked fish sample). Blue: $[M+H-H_2O]^+$ Orange: $[M+H]^+$ Grey: $[M+NH_4]^+$ Yellow: $[M+Na]^+$.

Figure A2: Concentration of fish sample spiked with 10, 20, 50, and 100 ppb of P-CTX3C standard after sample preparation and SPE versus peak intensity. Calibration solution 2 (prepared on a separate day from the spiked fish sample). Blue: $[M+H-H2O]^+$ Orange: $[M+H]^+$ Grey: $[M+NH4]^+$ Yellow: $[M+Na]^+$

List of Tables

List of Abbreviations

ACN: Acetonitrile CTX: Ciguatoxin

C-CTX: Caribbean Ciguatoxins

CFP: Ciguatera Fish Poisoning

Da: Dalton

EFSA: European Food Safety Authority

ESI: Electrospray ionization

EtOAc: Ethyl acetate

g: Gram

H_2O: Water

HPLC: High-Performance Liquid Chromatography

HRMS: High-Resolution Mass Spectrometry

I-CTX: Indian Ciguatoxins

ID: Inner Diameter

IS: Internal Standard

LC: Liquid chromatography

LC-MS/MS: Liquid Chromatography with Tandem Mass Spectrometry

LOD: Limit of detection

LOQ: Limit of quantitation

LRMS: Low Resolution Mass Spectrometry

MEF: Matrix Effect Factor

MeOH: Methanol

MS: Mass Spectrometry

MRM: Multiple Reaction Monitoring

MTX: Maitotoxin

N2: Nitrogen gas

N2A: Mouse neuroblastoma cells

NCE: Normalized collision energy ng: Nanogram

P-CTX: Pacific Ciguatoxins

P-CTX-3B: Pacific Ciguatoxin-3B

ppm: Parts per million

ppb: Parts per billion

QA/QC: Quality Assurance/Quality Control

R2: Coefficient of Determination (R-squared)

SD: standard deviation

S/N: Signal-to-noise ratio

SPE: Solid Phase Extraction

µL: Microliter

US FDA: United States Food and Drug Administration

WHO: World Health Organization

$[M+H]^{+:}$ Protonated molecule

$[M+NH_4]^+$: Molecule plus ammonium adduct

$[M+H-H_2O]^+$: Protonated molecule with water loss

$[M+Na]^+$: Molecule plus sodium adduct

1.0 General Introduction

1.1 Introduction to Ciguatera Fish Poisoning

Ciguatera Fish Poisoning (CFP) is a non-bacterial foodborne illness that is caused by consuming tropical and subtropical fish contaminated with a class of toxic compounds called ciguatoxins (CTX) (Friedman et al., 2008). CFP is currently the most common marine biotoxin disease effecting 50,000 people globally every year (Soliño & Costa, 2020). The number of people infected is believed to be under-reported because of the difficulty to make a firm diagnosis (Friedman et al., 2008).

CTXs are compounds naturally produced by epi-benthic dinoflagellates of the genus *Gambierdiscus and Fukuyoa* (Soliño & Costa, 2020). The same marine algae produce maitotoxin (MTXs) and gamberiol, related compounds to CTXs however, there is no direct evidence for their involvement in causing CFP (WHO 2018). CTX, MTX, and gamberiol are all bioactive molecules that contain cyclic ethers with variations in number of carbons, structure, and action of mechanism (Soliño & Costa, 2018).

The marine algae containing CTXs naturally grow and harbour along the coastal regions near coral reefs, therefore more episodes of CFP outbreaks occur along the coastline of the Caribbean Sea, Pacific, and Indian Oceans (Jiang et al., 2012). The CTXs from marine algae are ingested by herbivorous/omnivorous fish and transferred to carnivorous fish through grazing and predation, respectively (Sparrow & Heimann, 2016). CFP is generally associated with the consumption of predatory reef fish, such as barracuda. With

the tropical fish being distributed globally, cases can occur anywhere in the world (Figure 1.1) (Chinain et al., 2021). Studies for toxic benthic dinoflagellates started in the late 1970s, however, standardization methods for the confirmation and exploration of CTXs in marine organisms remain challenging due to limited standard availability (Moestrup 2015). Fish is a major food source and economic factor for many endemic communities and therefore CFP must be properly identified and managed to help protect residents' health and their economy (Chinain et al., 2019).

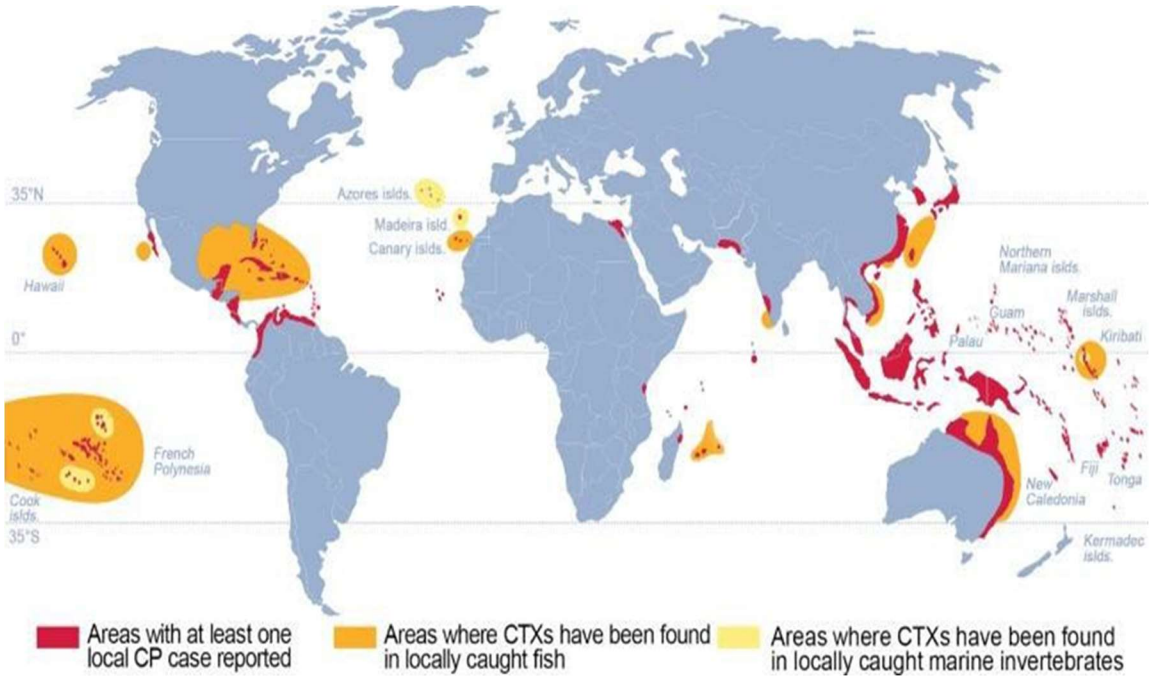

Figure 1.1: Regions with at least one local CFP case reported (red), CTXs confirmation in locally caught fish (orange) and marine invertebrates (yellow) (Chinain et al., 2021).

1.2 Chemistry of Ciguatoxins

CTXs contain contiguous cyclic ether rings fixed in a "ladder" design (Figure 1.2) and the two termini of the "ladder" are varied in congeners (Figure 1.2) (Pasinszki et al., 2020). There is also a large array of structurally related CTX congeners that are created through metabolism in fish (Friedman et al., 2008). Currently, 47 CTXs have been identified however, most have not been structurally characterized. CTX vary in the number of rings, backbone skeletons and geographical location which has allowed classifications in numerous categories (Pasinszki et al., 2020).

CTXs are based off three main CTX groups: CTX 1B, CTX 3C, and C-CTX-1. The common structure for the three derivatives consists of three main features: containing 13 rings where the last one (N) is non-contiguous and seen as a chain in M-seco analogues, a C5 side terminal chain and an E oxopene ring with 6 carbons and 1 oxygen atom. The main differences are on the sides of the molecule, R1 and R2 (Figure 1.2). These differences can be either changes in oxygen and methylene groups and/or present a higher number of oxygen atoms to one or both sides (Soliño & Costa, 2018).

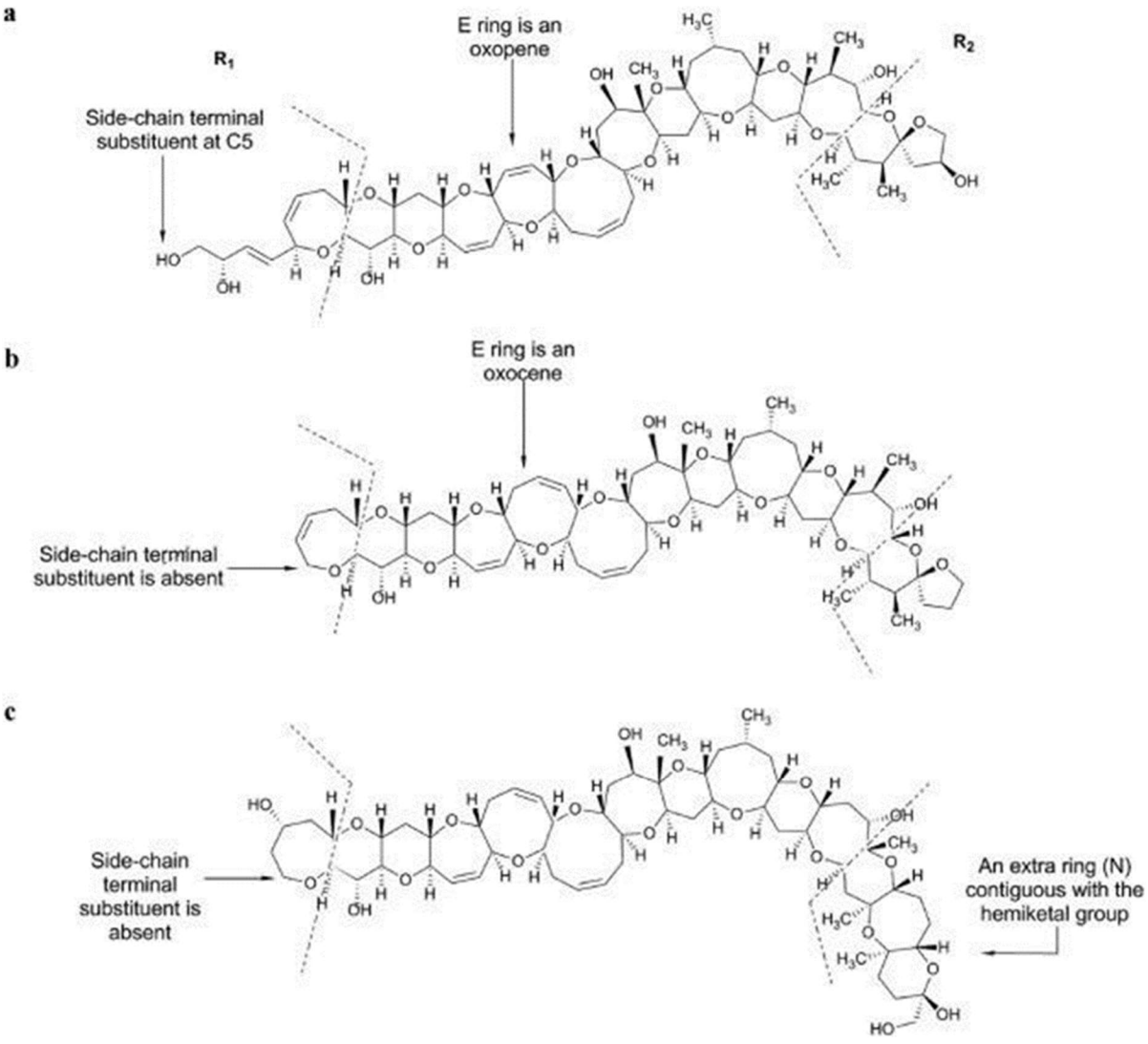

Figure 1.2: The structure and chemical features of the three derivatives of the main CTX groups: a) CTX1B, b) CTX3C and c) C-CTX-1 (Soliño & Costa, 2018).

CTXs have been further categorized depending on their region of occurrence: the Pacific Ocean (P-CTX), Caribbean Sea (C-CTX), and Indian Ocean (I-CTX) (Spielmeyer et al., 2022). Pacific CTXs are categorized into two groups, P-CTX-I (CTX1B type) and CTX3C type. CTX1B and CTX3C groups contain 13 rings with a main difference in the E ring and lack of the side-chain substituent in analogues from CTX3C type. The

Caribbean and Indian CTX have a structure similar to CTX3C type with an extra fused ring (C-CTX-1). The masses of P-CTX, C-CTX, and I-CTX congeners are summarized in Table 1.1. Presently, out of the 47 congeners, 22 CTX congeners have been identified in from Pacific fish samples (Figure 1.3). The congeners are differentiated by the sides of the molecule varying in the number of oxygen atoms. Epimers (diastereomers that differ in configuration by only one chiral center) are also included as a separate congener (Pasinszki et al., 2020).

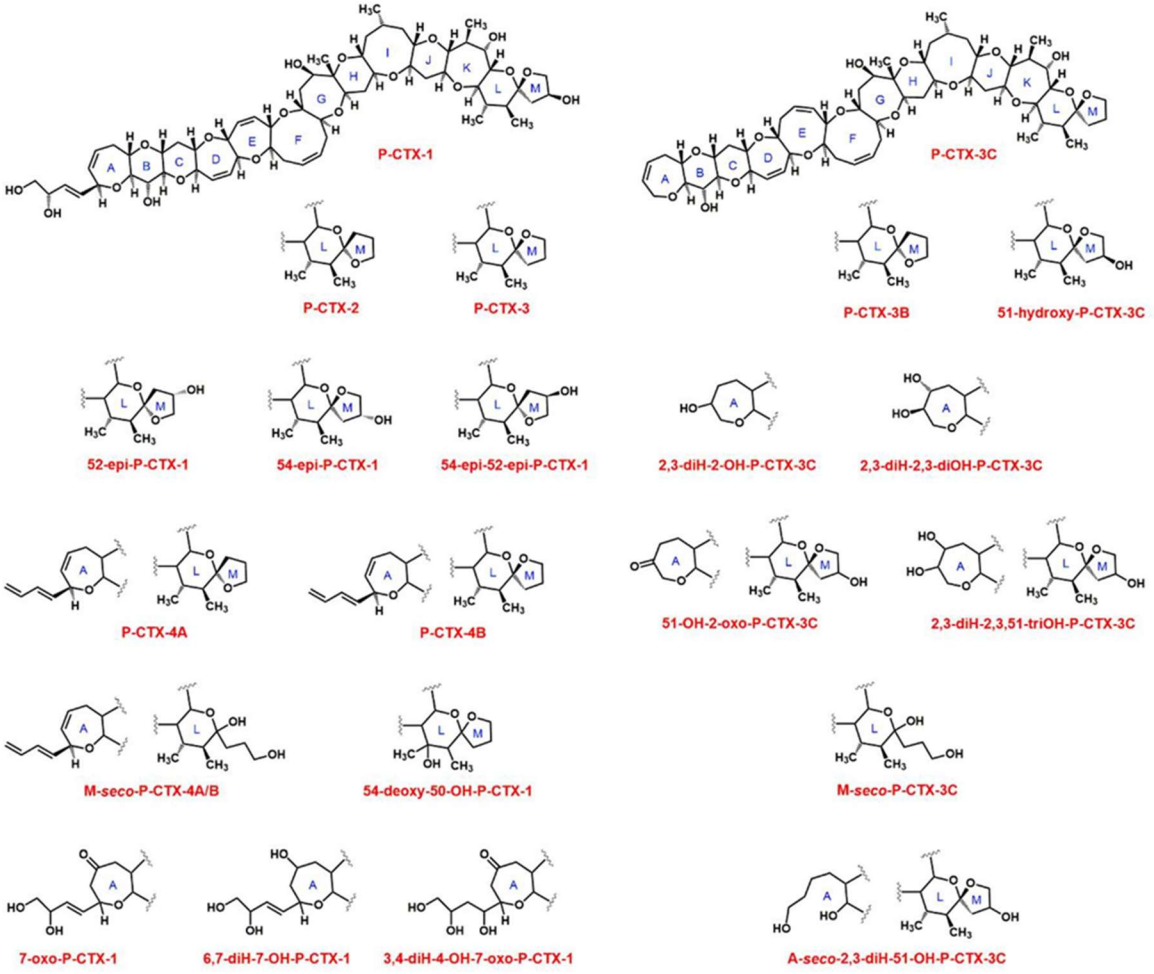

Figure 1.3: Structure of Pacific CTX congeners (Pasinszki et al., 2020).

Table 1.1: Molecular formula and mass (Da) of identified ciguatoxins (P-CTX, C-CTX, and I-CTX) (Pasinszki et al., 2020).

Pacific CTXs			**Caribbean CTXs**		
P-CTX-1	C60H86O19	1110.6	C-CTX-1 5	C62H92O19	1140.6
52-*epi*-P-CTX-1	C60H86O19	1110.6	C-CTX-2 5	C62H92O19	1140.6
54-*epi*-P-CTX-1	C60H86O19	1110.6	C-CTX-1141a	C62H92O19	1140.6
54-*epi*-52-*epi*-P-CTX-1	C60H86O19	1110.6	C-CTX-1141b	C62H92O19	1140.6
P-CTX-2 2	C60H86O18	1094.6	C-CTX-1141c	C62H92O19	1140.6
P-CTX-3 2	C60H86O18	1094.6	C-CTX-1127	C61H90O19	1126.6
7-oxo-P-CTX-1	C60H86O20	1126.6	C-CTX-1143	C62H94O19	1142.6
6,7-diH-7-OH-P-CTX-1	C60H88O20	1128.6	C-CTX-1143a	C62H94O19	1142.6
3,4-diH-4-OH-7-oxo-P-CTX-1	C60H88O21	1144.6	C-CTX-1157	C62H94O20	1156.6
54-deoxy-50-OH-P-CTX-1	C60H86O19	1110.6	C-CTX-1157a	C62H94O20	1156.6
P-CTX-3C 3	C57H82O16	1022.6	C-CTX-1157b	C62H94O20	1156.6
P-CTX-3B 3	C57H82O16	1022.6	C-CTX-1159	C62H93O21	1158.6
51-OH-P-CTX-3C	C57H82O17	1038.6			
2,3-diH-2-OH-P-CTX-3C	C57H84O17	1040.6	**Indian CTXs**		
2,3-diH-2,3-diOH-P-CTX-3C	C57H84O18	1056.6	I-CTX-1	C62H92O19	1140.6

Table 1.1: Molecular formula and mass (Da) of identified ciguatoxins (P-CTX, C-CTX, and I-CTX) (Pasinszki et al., 2020).

M-*seco*-P-CTX-3C	C57H84O17	1040.6	I-CTX-2	C62H92O19	1140.6
P-CTX-4A	C60H84O16	1060.6	I-CTX-3	C62H92O20	1156.6
P-CTX-4B	C60H84O16	1060.6	I-CTX-4	C62H92O20	1156.6
M-*seco*-P-CTX-4A/B	C60H86O17	1078.6	I-CTX-5	C62H90O19	1138.6
51-OH-2-oxo-CTX-3C	C57H82O18	1054.6	I-CTX-6	C62H90O20	
2,3-diH-2,3,51-triOH-P-CTX3C	C57H84O19	1072.6			
A-*seco*-2,3-diH-51-OH-P-CTX-3C	C57H86O18	1058.6			

- OH = hydroxy, H = hydro, n.a. = not available; [2,3,4,5] Epimers. Alternative or old names: P-CTX-1 = CTX-1B and CTX; P-CTX-2 = 52-*epi*-54-deoxy-CTX-1B; P-CTX-3 = 54-deoxy-CTX-1B; P- CTX-3B = 49-*epi*-P-CTX-3C; P-CTX-4B = 52-*epi*-P-CTX-4A, GTX-4B, GT-4B or gambiertoxin- 4B; 49-*epi*-P-CTX-3C = P-CTX-3B; 56-*epi*-C-CTX-1 = C-CTX-2; 2,3-dihydro-2,3-dihydroxy-P- CTX-3C = 2,3-dihydroxy-P-CTX-3C = CTX-2A1.

1.3 Biotransformation of Ciguatoxins

Accumulation of CTXs is hypothesized to occur from biotransformation, primarily oxidation, and acid-catalyzed spiroisomerization within the fish liver, likely facilitated by specific cytochrome P450 enzymes, although the precise identification of these enzymes remains unclear (Gwinn et al., 2021). This biological diversity process is believed to be

the source for the broad spectrum of CTX congeners observed (Spielmeyer et al., 2022). Studies have shown that the least oxidized CTX congeners are found in organisms at lower trophic levels, while higher trophic level organisms would contain the most oxidized CTX congeners (Lewis and Holmes, 1993; Murata et al., 1990; Satake et al., 1997; Scheuer et al., 1967). As CTXs are oxidized, metabolites become more polar and toxic. Therefore, the higher trophic level organisms by default would contain the most toxic CTX congeners (Murata et al., 1989), which also puts humans especially at risk as they typically eat fish at the top of the food chain.

Over 400 species of fish have been known to cause CFP (Rousseaux et al., 2013). Most of the species are carnivorous reef fish such as grouper, snapper, barracuda, jack, sturgeon, sea bass, and moray eel. Some herbivorous/ omnivorous fish may also cause CFP if eaten such as surgeonfish and parrotfish. Open ocean pelagic fish such as tuna and mahi-mahi have not been associated with causing CFP (Ansdell, 2019). Mak et al., 2013 has shown that various fish species may exhibit different capacities for CTX accumulation. The study found a dominance of P-CTX-2 in herb/omnivorous fish in comparison to P-CTX-1 being the most dominant species in carnivorous fish.

Although coral reef fish are regarded as the primary organisms causing CFP, ciguatera-like poisoning events after the ingestion of giant clams (*Tridacna maxima*), marine gastropods (*Tectus niloticus*), and sea urchins (*Tripneustes gratilla*) are occasionally reported. Research has found these organisms also bioaccumulate CTXs beyond the safety limit for human consumption (Roué et al., 2018). The effects of CTXs on marine

fauna are less documented, however exposure of CTXs was observed in fresh/brackish water species such as blueheads (*Thalassoma bifasciatum)* juveniles of *Oreochromis* sp., larvae and embryos of the genus *Oryzias*, and adult (*Mugil cephalus)* (Leite et al., 2021). Marine mammals may also suffer from CTX exposure according to a study observing CTX accumulation in the brain, liver, and muscles of stranded *Monachus schauinslandi* monk seals (Bottein et al., 2011).

CTXs bioaccumulate and bio-transform in the organs of an organism. Li et al., (2020) observed that the concentrations of total CTXs in the tissues of orange-spotted grouper (*Epinephelus coioides*) exposed to 1 ng P-CTXs per g of fish daily over a 30-day exposure generally increase in the order of liver, intestine, gill, skin, brain, and muscle. The study concluded the rising percentage of P-CTX-1 and the declining percentages of P-CTX-2 and -3 during the exposure phase indicated a probable transformation of P-CTX-2 and -3 into P-CTX-1. Continuous exposure of P-CTXs caused a linear increase while the depuration of P-CTXs from the body progressed with an exponential decrease (Li et al., 2020). This trend was also seen for other toxins such as natural phycotoxins (such as paralytic shellfish toxins, diarrhetic shellfish toxins, and azaspiracids) and synthetic organic chemicals (such as polybrominated diphenyl ethers) in marine organisms (Costa et al., 2011; Munschy et al., 2011; Jauffrais et al., 2012; Lopes et al., 2014; Nielsen et al., 2016). The study also observed that the fastest elimination route for CTXs is in the liver, whereas the elimination trends for the other five organs (brain, intestine, gill, skin, muscle) all varied with the skin and gills taking the longest to

eliminate the CTXs. This indicates that different tissues may have different processes to remove CTXs (Li et al., 2020).

The resistance mechanism in fish is still unknown, however, exposure to CTXs in laboratory settings may affect their fitness and, consequently, their survival rates. CTXs may trigger physiological and behavioral effects, like unsuccessful hatching, hyperkinetic twitching, caudal fin malformation, spinal abnormalities, and immune dysfunction. Laboratory studies have shown these effects to be potentially fatal to embryos of Japanese medaka (*Oryzias latipes*), larvae of marine medaka (*Oryzias melastigma*), and mosquito fish (*Gambusia affinis*) (Mak et al., 2017; Yan et al., 2017; Colman et al., 2004; Lewis, 1992; Yan et al., 2020; Edmunds et al., 1999). Therefore, CTX-sensitive species might be more susceptible to being preyed on by predators, that may affect the structure and function of the food web (Li et al., 2020).

1.4 Pathophysiology of Ciguatoxins

CTXs affect the central nervous system by binding to voltage-gated sodium channels in the axon of neurons (Dechraoui et al., 1999). When the neuron is at resting potential, no electrical signals are being sent, and therefore, the sodium channels are closed. CTXs open these sodium channels at resting potential, causing an influx of sodium and depolarizing the axonal membrane. Depolarizing the axonal membrane triggers spontaneous and repetitive action potentials (electrical signals) (Friedman et al., 2017). Under normal circumstances, an influx of sodium causes an efflux of potassium, maintaining electroneutrality within the axon and controlling the movement of water

across the membrane (Mattei et al., 2014). When CTX interrupts the influx/efflux process, it creates swelling in the nodes of Ranvier (myelin sheath gaps) (Benoit et al., 1997). This swelling impairs the saltatory conduction along the axon and slows down the conduction velocity of the electrical signals (Cameron et al., 1991; Cameron et al., 1991). These effects on the central nervous system likely contribute to the disturbance of sensory and motor skills observed in CFP, such as burning sensation in the hands and feet (paresthesia) and muscle weakness.

1.5 Ciguatoxin Safety Limit

The toxin that has been regarded as the most potent is P-CTX-1. The recommended safety limit for CTXs in fish for safe human consumption has been set to 0.01ng P-CTX-1 toxin equivalent per g of fish tissue (0.01 ppb P-CTX-1 equivalent). This limit is from both the European Food Safety Authority (EFSA) and United States Food and Drug Administration (US FDA) (U.S. Department of Health and Human Services, 2020). The recommended safety level for C-CTX-1 equivalent toxicity has been set to 0.10 ppb (Dickey & Plakas, 2010). The safety limit for I-CTXs has not been published yet however, research has indicated that the toxicity of I-CTX-1 is 60% of that of P-CTX-1 potency therefore, a safety level of 0.017 ppb for I-CTX equivalent toxicity may be considered (Hamilton et al., 2002).

1.6 Symptoms and Treatment of CFP

There are no diagnostic techniques for CFP, therefore health care institutions rely on the patient's history and characteristic symptoms. There have been up to 175 different

symptoms recorded in both acute and chronic phases of CFP (Wang, 2008). Due to the variety of symptoms that have been observed with patients with CFP, it makes it difficult for physicians to give a CFP diagnosis with full certainty (Friedman et al., 2017). CFP can be mistaken for other diseases since it can have similar symptoms to other fish poisonings and enteroviruses such as organophosphate toxicity, multiple sclerosis, Guillain-Barre syndrome and others (Gatti et al., 2008). Research in animal laboratories have shown that CTXs are absorbed directly into the gastrointestinal tract and distributed throughout the body (Dechraoui Bottein et al., 2011). Since CTXs influence voltage gated sodium channels, they can affect many systems in the body (brain, skeletal muscle, heart, peripheral nervous system, sensory neurons) and therefore mediate the symptoms of CFP (Friedman et al., 2017).

The most common clinical scenario for infected patients would be early gastrointestinal cardiovascular symptoms such as nausea, vomiting, and diarrhea that appear after 48 hours of eating the toxic fish (Friedman et al., 2017). Duration of such symptoms can range from several days to weeks, however depending on the amount of CTX and the frequency the body is exposed, symptoms can persist and become chronic. These first set of symptoms generally subside by itself within a few days, some symptoms mainly neurological (paresthesia, dysesthesia, asthenia, neurocognitive disorders) and psychiatric (anxiety, depression) can last for months or years in chronic cases (Chinain et al., 2021). CFP symptoms can also be revived from more consumption of certain marine-related substances (even in the absence of CTXs), meats, nuts, alcohol, or sometimes intense

physical activity, temperature variations, or stress (Lange, 1992; Fleming & Blythe, 1997; Lewis, 2001; Gatti et al., 2018).

Patients with CFP usually have symptoms that last a few days; however, patients should be advised to avoid eating fish and certain products and activities that may exacerbate the symptoms or cause a relapse. The health care for infected patients is significantly hampered by a lack of antidotes that can specifically cure CFP, and the medical management of acute and chronic symptoms of CFP. Patients rely mainly on case-by-case symptomatic support, and diet recommendations (Friedman et al., 2008).

1.7 Preventative strategies for CFP

The main management strategy for lowering CFP cases that are often practiced in ciguatera-endemic countries is to avoid eating commonly infected fish species. Fish processors are advised to not purchase or harvest fish from areas of known ciguatoxin activity. In CFP endemic regions, prohibitions against harvesting high-risk fish species have taken place (Friedman et al., 2017). The weight of the fish, fishing region, fishing activity (commercial versus sport fishing) as well as the season of the year are all risk factors that contribute to many communities CFP management (Acosta, 2015; Sanchez-Henao et al., 2019).

Residents in CFP-endemic countries have noticed higher ciguateric incidences in warmer sea water, especially in the warmer months where algal blooms are often observed (Tester et al., 2020). Locals would avoid all fishing activities during the warmer months

of the year to avoid the chance of getting CFP. Studies have shown global warming having an impact on the growth rate of ciguatoxin algae. As temperatures increase, we can expect some *Gambierdiscus and Fukuyoa* species to expand to latitudes further from the equator. This causes concern as seasonality being part of ciguatera management may not be as reliable due to the changing of climate (Chinain et al., 2021).

Other measures that help the prevention of CFP outbreaks are maintaining surveillance and reporting of CFP to public health agencies, education and outreach to consumers and professionals, and poison control center support (Friedman et al., 2017). In the US, news of outbreaks of CFP are reported from public health care officials to the Centers for Disease Control and Preventions (CDC) surveillance system and the National Outbreak Reporting system. In French Polynesia where CFP regularly occurs, it became an official notifying disease in the government surveillance program that is under the supervision of the Public Health Directorate (Chinain et al., 2010). Local poison control centers provided by the World Health Organization can give assistance to healthcare workers and physicians if a patient is suspected of having CFP (World Health Organization, 2017). Having residents and health care professionals report potential cases to local/ state health departments can help public health authorities investigate further in the case, identify outbreaks to notify the public, and can help prevent further CTX exposures (Friedman et al., 2017).

1.8 Identification of Ciguatoxins in Fish

Numerous methods for identifying CTX have been developed due to the serious health implications that CFP causes (Pasinszki et al., 2020). Unfortunately, ciguatoxins cannot be detected through taste, colour, or odor. They also survive heat and commercial freezing temperatures, therefore must be identified through experimentation (Lee et al., 2019). The methodologies used to identify ciguatoxins are mouse bioassays, biological methods (cytotoxicity assays, receptor-binding assays, and immunoassays), and chemical methods (HPLC with fluorescence detection through fluorescence labelling, LC-MS/MS). Many of these methods are limited in specificity, selectivity, and sensitivity for CTXs (Pasinszki et al., 2020).

Mouse bioassays involve purified samples injected into mice to observe signs of illness. This method contains numerous limitations such as tedious sample preparation, long waiting times, and poor sensitivity and specificity for a firm diagnosis (Friedman *et al.* 2008). It is expected to be replaced in labs due to the poor sensitivity and specificity, high cost, and the ethical and safety concerns (Pasinszki et al., 2020). The fluorescence-based receptor-binding assay (F-RBA) eliminates safety concerns associated with radioactive compounds required for radioimmunoassay. Due to testing kits being commercially available, this method is expected to increase in popularity. The most successful biological method thus far is the cell-based assay (CBA) using mouse neuro blastoma cells (N2A). This method is sensitive and simple to perform. However, it is time-consuming, observes only the combined effect of the CTX in the fish sample, and multiple toxins can block sodium channels. Immunosensors and immunoassays are

sensitive enough for CTX detection, however, are limited to the availability of CTX-antibodies. While theoretically, multiple toxins can be targeted simultaneously, assays usually incorporate only one or a very limited number of antibodies. Consequently, these methods fail to offer insights into toxin profiles (Pasinszki et al., 2020).

Immunosensors and immunoassays exhibit sensitivity adequate for CTX detection. Nevertheless, their effectiveness is constrained by the accessibility of CTX-specific antibodies and their inability to offer comprehensive toxin profiles, as multiple toxins cannot be concurrently targeted (Pasinszki et al., 2020).

Presently, CBA-N2A, F-RBA, and immunoassays are sensitive detection methods, however, they do not help with identifying the toxins' profile. CTXs must be separated and analyzed individually since they do not have characteristic functional groups for spectroscopic detection, and HPLC is the most popular and preferred choice. However, UV detectors are not sensitive enough to detect the small concentrations that CTXs are usually found in. There is also a lack of chromophores that can be used for detection (Caillaud et al., 2010; Lewis et al., 1991; Vernoux & Lewis, 1997; Lewis & Sellin, 1992). Fluorescent labeling can be used targeting the CTX primary hydroxyl group located at the terminus. HPLC with fluorescent detection can be accomplished using 1-anthrylcarbocyanide and carbonyl azides or carbonyl nitriles of coumarin derivatives as labels. This method was observed to be more sensitive than HPLC-UV, but it still could not detect the recommended requirement tolerance level 0.01ng g-1 for P-CTX-1 (Caillaud et al., 2010; Yasumoto & Satake, 1996; Yasumoto et al., 1995). Another

limitation would be that herbivores containing CTX have little abundance of the primary hydroxyl group, making CTX difficult to detect using HPLC-UV (Legrand et al., 1992). The first time HPLC was used with tandem mass spectrometry (HPLC -MS/MS) to detect CTXs was in 1994 by Lewis and Jones (1997). The technique detected as little as 0.04 ppb for P-CTX-1 and 0.1 ppb for C-CTX-1, using gradient reversed-phase HPLC and an electrospray triple quadrupole mass spectrometer (Lewis et al., 1998). HPLC coupled with MS/MS allowed a more sensitive detection compared to fluorescence detection and quickly became the most prominent technique for CTX detection. The technique was able to accurately perform separation and identification of CTXs plus it provided toxin profiles. The technique, however, still needs reference standards (Pasinszki et al., 2020).

Molecular peaks and fragmentation can provide a lot of information for the detection of CTXs. However, the fragmentation pattern is mostly made up of water losses where results differ from instrument to instrument and therefore, a diagnostic fragmentation pattern may not always be achieved. A biological assay is typically combined with LC-MS/MS for confirmation of CTXs in biological materials. Raw fish extracts can be used with LC-MS/MS but must be purified through SPE to remove fatty acids and lipids that can interfere with MS analysis. Matrix-co extractives greatly interfere with the ionization causing signal suppression (Harwood et al., 2017). To achieve low limits of detection both HPLC and MS conditions should be optimized for sensitivity and selectivity. The conditions that should be optimized are the LC conditions, ionization sources, ion monitoring choices and acquisition modes (Yogi et al., 2011; Murray et al., 2018; Sibat et al., 2018, Moreiras et al., 2018). Various analytical protocols have been compared using

LC-MS/MS and HRMS (Sibat et al., 2018). This study will be frequently referring to the Sibat et al., (2018) study to compare methodologies and results.

LC/MS techniques, particularly LC tandem mass spectrometry with triple quadrupole instruments, offer greater sensitivity than HRMS. On the other hand, HRMS, such as Time of Flight and Orbitrap spectrometers, provide the molecular formula and isotopic information of CTX, facilitating better identification of CTX analogues (Sibat et al., 2018; Suzuki et al., 2017). HRMS offers advantages in avoiding false positives, especially at higher concentrations or in the absence of reference material, while the low mass accuracy of LC-MS/MS increases the risk of misidentification. An example of P-CTX3C interference in low resolution tandem mass spectrometry LRMS/MS was demonstrated using a *Gambierdiscus* culture from Southwater, USA (Sibat et al., 2018). The same study observed that HRMS excels in identifying interferences caused by unknown co-eluting compounds. It was discussed that a specific peak observed in a *Gambierdiscus* spp. strain, resembling authentic P-CTX3C, would be incorrectly attributed to P-CTX3C when using LRMS. This misattribution was confirmed in full scan HRMS analysis, revealing substantial differences in MS spectra patterns and accurate mass (Sibat et al., 2018), HRMS has also been instrumental in identifying new ciguatoxins, such as the recent discovery of C-CTX-5C using LC-HRMS (Mudge et al., 2023; Pottier et al., 2023). LC-HRMS, especially when coupled with a reference standard, is recommended for CTX identification. Overall, LC-HRMS is both selective

and sensitive enough to detect CTX at the tolerance limit, surpassing other confirmatory methods (Pasinszki et al., 2020).

1.9 Research Problems

Detecting ciguatoxins (CTXs) in biological material poses considerable challenges due to their low concentrations, the presence of various CTX congeners, limited or absent CTX standards, the co-occurrence of interfering compounds in fish tissue, and the difficulty in collecting CTX-infected samples due to the unpredictable nature of CTX incidences (Pasinszki et al., 2020). Unlike many other marine biotoxins causing food poisoning, there is currently no standardized method for CTX detection. Consequently, only a few methods utilizing an LC-MS/MS protocol have been developed, which offers sufficient sensitivity and selectivity for identifying CTX, with even fewer options for LC-HRMS. Although LC-MS/MS is the most common method used, suggestions have been made that utilizing LC-HRMS with a reference standard would be the optimal choice for the most accurate identification of CTXs (Sibat et al., 2018).

1.10 Study Objectives

This study distinguishes itself through its utilization of HRMS, including a detailed optimization of analytical parameters. Furthermore, it focuses on the P-CTX-3B analogue, which previously has not been studied in any detail. Finally, it offers a forward- looking perspective on future research challenges and directions. The primary goal of this study is to develop a more sensitive analytical method for detecting CTX

utilizing HRMS, addressing the challenges associated with CTX detection. The approach involves optimizing conditions that influence the fragmentation and formation of CTX ions. It systematically evaluates critical parameters, such as proper solvents, collision energy, and flow rate to identify the optimal conditions for the analysis. Eventually, the developed method is applied to a fish sample spiked with P-CTX-3B to validate the analytical conditions within the complex matrix of fish tissue. The calibration curve generated from CTX-spiked fish samples serves as a crucial aspect of this validation process. These unique aspects contribute to a more comprehensive understanding of CTX detection methodologies and pave the way for the development of improved techniques in the field of ciguatera detection.

CHAPTER 2 – Method Development: ESI Optimization for Ciguatoxin Standard

2.1 Introduction

This chapter utilizes a CTX standard to refine ionic conditions crucial for ionization efficiency, focusing on solvent chemistry, flow rate, and collision energy. To determine these optimal conditions, the limits of detection (LOD), limits of quantitation (LOQ), and mass accuracies were calculated and evaluated. The CTX was examined in two different solutions and directly infused into the mass spectrometer for analysis.

2.1.1 Ion Response Optimization

Mass spectrometry has become one of the most preferred analytical techniques for CTX identification due to its high sensitivity and selectivity. Sensitivity can be expressed as

the signal-to-noise ratio (S/N) (Ingle, 1974), which is defined as the ratio of signal intensity (S) to noise (N) obtained for a certain amount of sample (Gross, 2011). Therefore, increasing the signal intensity or decreasing the noise will improve the sensitivity of the method. A greater S/N typically indicates better sensitivity for the analyte. In addition, the LOD and LOQ can also be used to express sensitivity. The LOD is the lowest concentration of the analyte that is reliably detected in the sample at an S/N of 3 and the LOQ refers to the concentration at which a target analyte is not only detected but also reliably quantified at an S/N of 10 (Nijat et al., 2020). Lower LOD and LOQ usually reflect higher sensitivity of the respective mass spectrometers (Li et al., 2021). Often, sensitivity directly relates to ionization efficiency, which is the effectiveness of forming gas-phase ions from analytes in solution and transmission efficiency which is the ability to transfer formed ions from atmospheric pressure to the low-pressure zone of the MS system (Page et al., 2007). Ionization efficiency is strongly influenced by flow rate, mobile-phase composition, co-extractives and the physicochemical properties of the target analytes. The easiest and most effective method to improve sensitivity is through optimization of the ionization source to ensure maximum production and transfer of gas phase ions into the MS system (Fekete, 2021).

2.1.2 Solvent Chemistry Optimization for CTX

Most of the solvents used for chromatographic separation for CTX detection using mass spectrometry were acetonitrile/water (ACN/H_2O) or methanol/water (MeOH/H_2O). It was not understood whether methanol or acetonitrile was preferred for the identification of CTXs (Sibat *et al.* 2018). This study compares the two solvents with their impact on the

ions predominant in the MS spectrum. There were multiple options for mobile phase additives such as sodium acetate and acetic acid however, the additives most used were formic acid and ammonium formate (Sibat *et al.* 2018). Sibat et al. (2018) used formic acid as a mobile phase additive in which the sodium adduct was favored in both methanol and acetonitrile solvents. However, they aimed to avoid the use of the sodium adduct due to its stability, which made fragmentation challenging. Therefore, in order to achieve MS/MS fragmentation, they tried to prevent the formation of sodium adducts. They did this by using ammonium formate to enhance the formation of ammonium and protonated adducts. In another study by Wu et al. (2011), it was noted that due to the abundance of $[M + Na]^+$ ions, P-CTX-1 was dissolved in a solution containing 50% aqueous acetonitrile with 1% formic acid and 30 mM ammonium formate. This solution was specifically designed to encourage the formation of preferred precursor ions, $[M + NH_4]^+$ and $[M + H]^+$. Direct injection of P-CTX-1 in this sample matrix improved the intensity of $[M + NH_4]^+$ and was chosen as the precursor ion for P-CTX-1 characterization.

2.1.3 Collision Energy Optimization for CTX

Collision energy is an instrument parameter that is usually optimized to increase fragment ion intensity during HRMS (MacLean et al., 2010). The decision in collision energy can largely affect the successful identification of molecules in MS and therefore should be optimized (Révész et al., 2018). The normalized collision energy (NCE) values in most literature to detect CTX were between 10 eV and 40 eV (Sibat *et al.* 2018, Wu et al., 2011, Yon et al., 2021, Ramos-Sosa et al., 2022) For good fragmentation, it is desirable to have a strong precursor ion signal and well-resolved product ions with high signal-to-

noise ratios in order to obtain accurate and reliable mass spectra. Usually, the precursor ion should be approximately 1/3 of the product ion's signal intensity for satisfactory fragmentation (Rockwood et al. 2018).

2.1.4 Importance of Mass Accuracy

Mass accuracy is the discrepancy between the measured mass of an ion and its true mass. It serves as a vital metric in mass spectrometry, offering insights into measurement quality and instrument performance. High mass accuracy implies close alignment between the measured and true mass, reflecting precision and accuracy in the instrument (Gross, 1994). Conversely, low mass accuracy indicates a significant disparity, signaling lower instrument precision.

In various mass spectrometry applications, such as compound identification and elemental composition determination, accurate mass measurements play a pivotal role. A heightened mass accuracy enhances confidence in compound identification by minimizing the risk of misidentification based on slight mass differences. Furthermore, precise mass measurements facilitate the calculation of a compound's elemental composition, a critical step in structural elucidation (Brenton & Godfrey, 2010).

2.2 Materials and Methods

2.2.1 Standard and Chemicals

The ciguatoxin chosen for this experiment was 49-epi-CTX3C (CTX3B) provided by Dr. Mireille Chinain, Institut Louis Malardé (IRD), Tahiti, French Polynesia. The CTX3B was dissolved in 500 µL methanol solution (2 ng/µL). The standard was stored at a chilled temperature of 4°C until use.

The chemicals for the solvent solutions are HPLC grade methanol, HPLC grade acetonitrile, and HPLC grade ammonium formate, all purchased from Fisher Scientific and formic acid (88% purity) purchased from Sigma-Aldrich. High purity 18.2 MΩ cm^2 water produced at the Water Quality Centre, Trent University was also used.

2.2.2 Preparation of Solvent Solutions

Two solvent solutions were made to enhance ion formation of the standard during HRMS analysis. These solvent solutions were prepared to evaluate the ionization efficiency for the target analytes directly infused into the HRMS. Solvent A contained 100 mL of 50% acetonitrile: water (v/v), 0.1% formic acid, 5 mM ammonium formate and tested to have a pH 2. Solvent B contained 100 mL of 50% methanol: water (v/v), 0.1% formic acid, 5 mM ammonium formate and set to pH 2. The mass to make 5 mM of ammonium formate for a 100 mL solution was calculated to be

31.528 g.

To evaluate the ionization efficiency for the target analyte that is directly infused into the HRMS the following solutions were prepared. Ammonium formate (31.5 mg) was placed into each of two 100 mL beakers. A volume of 100 µL of formic acid was added to both beakers. The 50% acetonitrile: water solution was added to the first beaker and 50% methanol: water solution to the second beaker to make up the 100 mL solution. Both solutions were stirred using a magnetic stirrer (PC-353 Stirrer, Corning Glass Works) until ammonium formate was dissolved. Both solutions were checked for their pH using a pH meter (IQ150, IQ Scientific Instruments) and tested to have a pH 2.

2.2.3 Preparation of Standard Solutions

The concentration of the commercial standard CTX3B was 2 ng/µL or 2000 ppb. Two 200 µL standard solutions were created, one using solvent A and the other with solvent B. Both standard solutions were created by adding 10 µL of standard to get a total of 200 µL solution with a concentration of 100 ppb. Both standard solutions were made on the day of HRMS analysis.

2.2.4 Instrumentation and Set-Up

The instrument used for analysis was the Thermo Scientific QExactive Orbitrap mass spectrometer equipped with a heated electrospray ionization source (HESI) and syringe pump (Thermo Fisher Scientific). To minimize volumes, the syringe pump was placed as close as possible to the inlet of the ESI probe, requiring only a short length of tubing (polyetheretherketone, PEEK, 45 cm, 0.005”/0.13mm ID) (Figure 2.1).

Figure 2.1: Syringe pump set up for HRMS analysis.

2.2.5 HRMS Analysis

Solvent A and B blanks were infused into the Orbitrap directly via a 250 µL syringe (SGC Engineering, Fisher Scientific) and their mass spectra was acquired before their respective standard was analyzed. Mass spectrometric detection was performed in positive ionization mode (ESI using either full scan mode or tandem mass spectrometry (MS2)). The precursor ions of interest are *m/z* 1023.56756 $[M+H^+]$, *m/z* 1045.5495 $[M+Na]^+$, and *m/z* 1040.59411 $[M+NH_4]^+$ and were isolated using a width of 0.2 *m/z* for all MS2 analysis. Both standard solutions mass spectra were acquired in full scan mode and MS2 with a flow rate 5 µL/min for 1 minute. The mass range acquired was *m/z* 100-1500, at a resolution of 17,500. The sheath gas flow rate was 10 µL/min, the auxiliary gas flow rate was 0 µL/min, the sweep gas flow rate was 0. The capillary temperature was 320°C and the spray voltage was 3.30 kV.

The standards' mass spectra were acquired at different syringe flow rates of 1, 5, and 10 µL/min under full scan mode via a 100 µL syringe (SGC Engineering, Fisher Scientific) for 1 minute. With the standard containing solvent A, 3 additional mass spectra for each flow rate were acquired. Due to limited standard, replicate recording of mass spectra for solvent B was not possible.

Mass spectrometric determination of the sample dissolved in solvent A was performed using MS2. Precursor ions corresponding to $[M+H]^+$, $[M+Na]^+$, and $[M+NH_4]^+$, were selected for fragmentation using a *m/z* window of +/- 0.2 and a syringe flow rate of 5 µL/min, normalized collision energy (NCE) of 15 eV and acquired for 1 minute. Three

mass spectra of the standard in solvent A were acquired with normalized collision energy (NCE) values of 10 eV, 15 eV, and 20 eV for fragmentation of $[M+Na]^+$ at a flow rate of 5 µL/min for 1 minute.

Mass spectrometric determination of the standard in solvent B was performed using MS2 for the fragmentation of the ion corresponding to $[M+Na]^+$ and a syringe flow rate of 5 µL/min, NCE of 15 eV and acquired for 1 minute. Two additional mass spectra of the standard containing solvent B were acquired with NCE values of 10 eV and 15 eV Data processing and analysis were conducted using Thermo Xcalibur software (4.1.31.9). After each use of the Orbitrap, the capillary tube was cleaned using an HPLC pump (VP Liquid Chromatograph, Shimadzu). The cleaning was done with a flow rate of 1 mL/min for 10 minutes using 50% methanol in acetonitrile.

2.3 Results and Discussion

2.3.1 Solvent Chemistry

The mass spectra for P-CTX-3B shown in Figures 2.2 and 2.3 were obtained using positive ionization under full scan mode *m/z* 1000-1050. For both solvent A and Solvent B standard solutions, $[M+H]^+$ was the most abundant ion. Following the protonated molecule, $[M+NH_4]^+$ and $[M+H-H_2O]^+$ were also highly abundant. The lowest abundant ion was the $[M+Na]^+$ out of the precursor ions for P-CTX-3B. Solvent B had the highest peak intensities of $[M+H-H_2O]^+$ and $[M+Na]^+$ compared to Solvent A which had higher peak intensities for $[M+H]^+$ and $[M+NH_4]^+$. The highest peak intensity overall being 8.07E+04 from the ACN/H_2O standard solution for the protonated molecule.

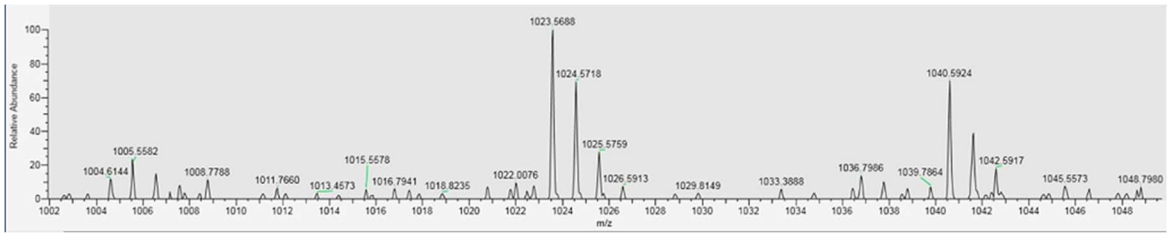

Figure 2.2: Mass spectrum of P-CTX3B in solvent solution containing ACN/H_2O acquired in positive full scan mode, at 100 ppb.

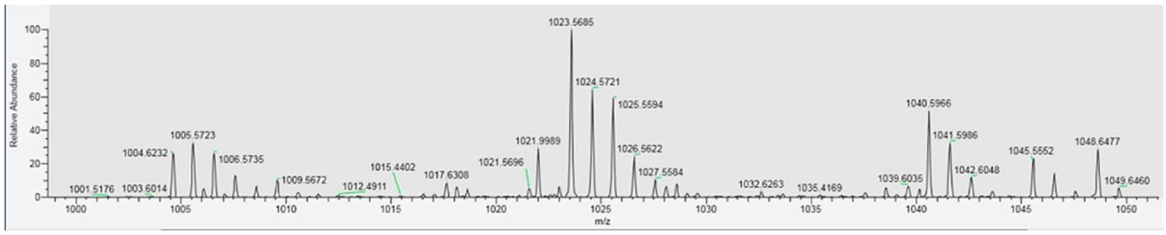

Figure 2.3: Mass spectrum of P-CTX3B in solvent solution containing MeOH/H_2O acquired in positive full scan mode, at 100 ppb.

The protonated molecule seemed to be the best choice to select for MS/MS as it was the most abundant ion. Pasinszki et al. (2020) also found that monitoring the protonated molecule usually exhibited lower signal-to-noise ratios compared to the ammonium or sodium adducts. They showed that it is depended on not only the LC and MS conditions, but also on the analyzed CTX. They found that the sodium and ammonium adducts were favoured when analyzing P-CTX-1B, whereas the ammonium adduct and protonated molecule were dominant for P-CTX-3C. Both CTXs were analyzed with similar intensities under the same LC conditions. Previous studies also used the protonated ion

for MS/MS fragmentation and found it to be the most abundant ion (Sibat et al. 2018; Wu et al. 2011).

A few studies reported that methanol-based mobile phases gave a better selectivity and sensitivity for detecting CTX (Sibat et al. 2018). The determination of the solvent may be indicative of the instrument used along with the method as some sources had better sensitivity and selectivity than others. For example, Sibat et al. 2018 used a time-of-flight mass spectrometer, and preferred methanol. Other studies have chosen to use acetonitrile due to methanol increasing the formation of highly stable $[M+Na]^+$ and found it difficult to fragment (Estevez et al. 2019; Estevez et al. 2020). Therefore, the proper selection of eluents and additives are important for CTX analysis especially for MS fragmentation.

2.3.2 Mass Accuracy

Tables 2.1 and 2.2 outline the accurate masses (both theoretical and measured) of ions originating from P-CTX-3C in standard solutions solvent A and solvent B, respectively. Although the ions under comparison are derived from P- CTX-3C rather than the standard analyzed in this study (C-CTX-3B), they are anticipated to closely resemble the ions expected in the mass spectrum of P-CTX-3B. A mass accuracy < 5 ppm would allow a confident identification of peaks shown in the mass spectrum differentiating between analyte and standard matrix or interferences. This is determined by comparing the theoretical mass of analyte peaks with actual peaks shown in the mass spectrum of the standard solution. Better mass accuracy allows more reliable peak assignments. In general, the acceptable value of the measured mass should be within 5 ppm of the

expected true mass (Gross 1994). The peaks that are far from the true mass or have a mass accuracy > 5 ppm cannot be confirmed with sufficient certainty. Due to this, the ions $[H\text{-}H_2O+H]^+$ (*m/z* 1005.56794), $[M+H]^+$ (*m/z* 1027.57852), $[M+NH_4]^+$ (*m/z* 1041.59747), and $[M+Na]^+$ (*m/z* 1045.55915) from solvent A, cannot be identified originating from P-CTX-3B with strong confidence. Both $[H\text{-}H_2O+H]^+$, and $[M+H]^+$ and two isotopes (*m/z* 1025.57427, 1026.57763, 1027.57852), from solvent B, cannot be identified originating from P-CTX-3B with strong confidence. This result is unlike other studies where most of the mass accuracy values were < 5 ppm (Sibat et al. 2018).

It was observed that ACN/H_2O provided greater accuracy and precision for the protonated adducts and methanol allowed greater accuracy and precision for the sodium adducts for this method. This observation agrees with other studies in which methanol was used to promote the formation of sodium adducts and acetonitrile was used to promote the formation of protonated molecules or ammonium adducts (Spielmeyer et al. 2021; Estevez et al., 2019; Yogi et al. 2011). This may be due to the solvents properties where methanol is a polar protic solvent donating protons and forming hydrogen bonds. In contrast, acetonitrile is a polar aprotic solvent that does not donate protons but can form dipole-diploe interaction with polar molecules. The methanol is likely forming strong ion-dipole interactions with the sodium ion. In acetonitrile, the ciguatoxins form protonated and ammonium adducts due to the weaker dipole interactions and hydrogen bonding (Jakob et al. 2021). It's important to note that the water content of 50% in the calibration solution could influence the outcome, suggesting that the previously mentioned solvent properties may not be the sole determining factors in choosing one

solvent over the other. From this study, it is suggested that methanol is better in forming sodium adducts versus acetonitrile which favors the formation of protonated and ammonium adduct for a more sensitive and selective identification of ciguatoxins.

Table 2.1: Accurate masses (theoretical and measured) of informative ions of P-CTX3B in solvent solution containing ACN/H_2O.

Ion	**Theoretical (*m/z*)**	**Measured (*m/z*)**	**Mass accuracy (ppm)**	**Peak height**
[M+H-H_2O]$^+$	1005.55253	1005.56794	15.32	1.85E+04
	1006.55588	1006.56815	12.19	1.16E+04
[M+H]$^+$	1023.56756	1023.56921	1.61	8.07E+04
	1024.57092	1024.57195	1.01	8.07E+04
	1025.57427	1025.57795	3.59	2.05E+04
	1026.57763	1026.58026	2.56	4.44E+03
	1027.57852	1027.58583	7.11	3.62E+02
[M+NH_4]$^+$	1040.59411	1040.58935	-4.57	5.43E+04
	1041.59747	1041.59064	-6.56	3.47E+04
	1042.60082	1042.59864	-2.09	1.16E+04
	1043.60418	1043.60259	-1.52	1.89E+03
	1044.6057	1044.60915	3.30	1.16E+03
[M+Na]$^+$	1045.54951	1045.55915	9.22	5.86E+03
	1046.55286	1046.57124	17.56	2.18E+03

Table 2.2: Accurate masses (theoretical and measured) of informative ions of P-CTX3B in solvent solution containing methanol.

Ion	Theoretical (*m/z*)	Measured (*m/z*)	Mass accuracy (ppm)	Peak height
[M+H-H2O]+	1005.55253	1005.57233	19.69	6.34E+04
	1006.55588	1006.57346	17.47	1.67E+04
[M+H]+	1023.56756	1023.56855	0.97	6.35E+04
	1024.57092	1024.5721	1.15	4.08E+04
	1025.57427	1025.55942	-14.48	3.76E+04
	1026.57763	1026.5622	-15.03	1.55E+04
	1027.57852	1027.55835	-19.63	6.60E+03
[M+NH4]+	1040.59411	1040.59657	2.36	3.26E+04
	1041.59747	1041.59858	1.07	2.06E+04
	1042.60082	1042.60476	3.78	7.49E+03
	1043.60418	1043.60672	2.43	2.27E+03
[M+Na]+	1045.54951	1045.55516	5.40	1.48E+04
	1046.55286	1046.55904	5.91	9.12E+03

2.3.3 Limit of Detection (LOD) and Limit of Quantitation (LOQ)

Table 2.3 presents the instrumental limits of detection (LOD) and limit of quantitation (LOQ) for P-CTX-3B ions in aqueous solution containing ACN/H2O at 100 ppb. Meanwhile, Table 2.4 provides a comparison between the peak heights of P-CTX-3B ions and the LOD and LOQ values in the same solution. The Limit of Detection (LOD) is defined as the lowest analyte concentration that can be reliably distinguished from the blank and is calculated as the average blank value plus 3 times the standard deviation (SD). Consequently, an analyte is considered detected once its signal response surpasses the LOD (Armbruster & Pry, 2008). To assess the method's reliability, the peak heights

for each ion were compared with the LOD to determine if the peak can be confidently differentiated from the blank. The most intense ions $[M+H-H_2O]^+$, $[M+H]^+$, $[M+NH_4]^+$, and $[M+Na]^+$ were all found to be above the LOD, indicating the standard's response is significantly above the noise level. Moreover, the Limit of Quantitation (LOQ) is described as the minimum concentration of an analyte that can be accurately and precisely detected. It is calculated as the average blank value plus 10 times the standard deviation (SD) (Lappas & Lappas, 2016). Furthermore, the peak intensities for each ion were compared with the LOQ to establish the concentration threshold—the point at which quantifying the analyte becomes challenging due to the proximity of the signal to the background noise. All ions, except for sodium ion, were found to be above the LOQ. Therefore, these ions, excluding sodium, can be reliably detected at a concentration of ppb.

Table 2.3: Average, standard deviation, limit of detection and limit of quantitation of P-CTX-3B most intense ions in the ACN/H_2O blank solution (n = 3).

Blank	**Peak Height**			
	$[M+H-H_2O]^+$	$[M+H]^{\pm}$	$[M+NH_4]^{\pm}$	$[M+Na]^{\pm}$
Run 1	6.51E+02	3.18E+03	2.39E+03	2.77E+02
Run 2	2.30E+01	7.53E+01	1.33E+01	8.36E+01
Run 3	1.78E+03	6.30E+03	1.96E+03	2.12E+03
Average	8.18E+02	3.19E+03	1.45E+03	8.27E+02
SD	8.90E+02	3.11E+03	1.27E+03	1.12E+03
LOD	3.49E+03	1.25E+04	5.25E+03	4.20E+03
LOQ	9.72E+03	3.43E+04	1.41E+04	1.21E+04

Table 2.4: Comparison of P-CTX-3B ions peak height (standard solution containing acetonitrile at 100 ppb) with the limit of detection and limit of quantitation of the blank containing acetonitrile.

Ions	**Peak height**	**LOD**	**LOQ**
$[M+H-H_2O]^+$	1.85E+04	> LOD	> LOQ
$[M+H]^{\pm}$	8.07E+04	> LOD	> LOQ
$[M+NH_4]^{\pm}$	5.43E+04	> LOD	> LOQ
$[M+Na]^+$	5.86E+03	> LOD	< LOQ

2.3.4 Fragmentation Study (MS2)

Collision energy affects the successful identification of molecules in MS/MS, with normalized collision energy (NCE) values between 10 and 40 eV commonly used for detecting CTX's (Sibat et al., 2018; Wu et al., 2011; Yon et al., 2021; Ramos-Sosa et al., 2022). Optimizing collision energy is crucial for enhancing fragment ion intensity, ensuring accurate and reliable mass spectra. Effective fragmentation requires a strong precursor ion signal and well-resolved product ions with high signal-to-noise ratios, ideally with the precursor ion around 1/3 of the height of the product ion (Rockwood et al. 2018). The ion $[M+H]^+$ was selected to fragment due to its higher intensity. Figures 2.4, 2.5, and 2.6 show Solvent A fragments that were observed at NCE values of 10, 15, and 20 eV, respectively and each scan acquired for 1 minute. Figures 2.7 and 2.8 show Solvent B fragments that were observed at NCE values of 10 and 15 eV, respectively. The NCE value that provided strong fragments for Solvent A was 15 eV. The product ions were differentiated from the noise and the precursor ion $[M+H]^+$ was still visible. At 10 eV it was observed that there was not a lot of product ions due to the precursor ion not being fragmented enough. At 20 eV it was observed that the precursor ion was not visible due to the many product ions that were formed and were hard to distinguish from the noise. Solvent B did not produce a strong fragmentation pattern. It was observed that 10 eV did not fragment the ion enough due to the strong precursor ion signal and hardly any product ions formed that were distinguishable from the noise. It was observed that 15 eV fragmented the precursor ion too much where the product fragments could not be distinguished from the noise.

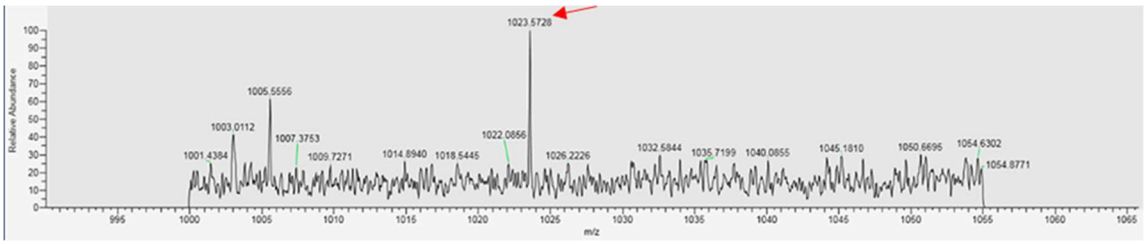

Figure 2.4: Mass spectrum of P-CTX3B in solvent solution containing ACN/H_2O acquired in MS/MS scan mode for 3 mins, selected ion *m/z* 1023.57852, collision energy at 10 eV, at 100 ppb.

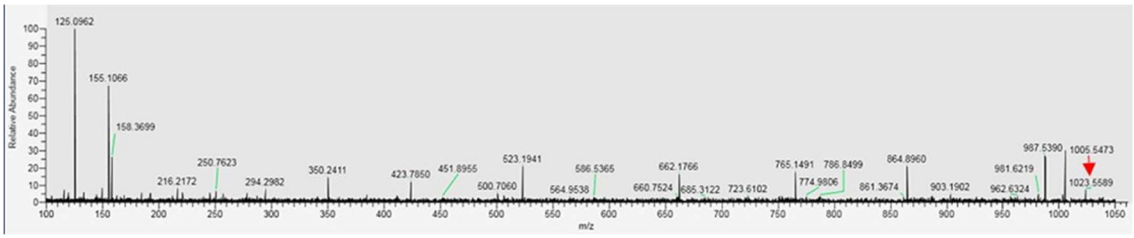

Figure 2.5: Mass spectrum of P-CTX3B in solvent solution containing ACN/H_2O acquired in MS/MS scan mode for 3 mins, selected ion *m/z* 1023.57852, collision energy at 15 eV, at 100 ppb.

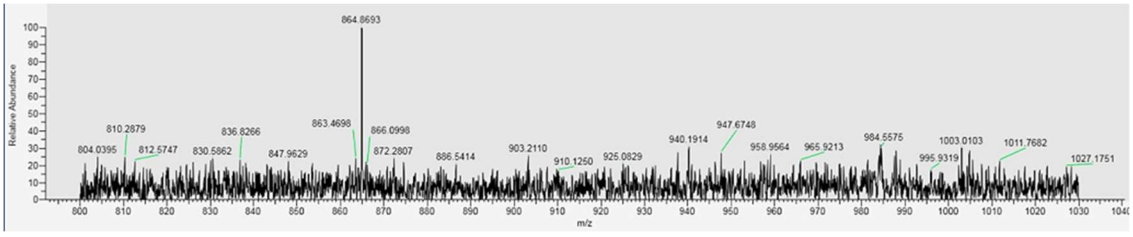

Figure 2.6: Mass spectrum of P-CTX3B in solvent solution containing ACN/H_2O acquired in MS/MS scan mode, selected ion being *m/z* 1023.57852, collision energy at 20 eV, at 100 ppb.

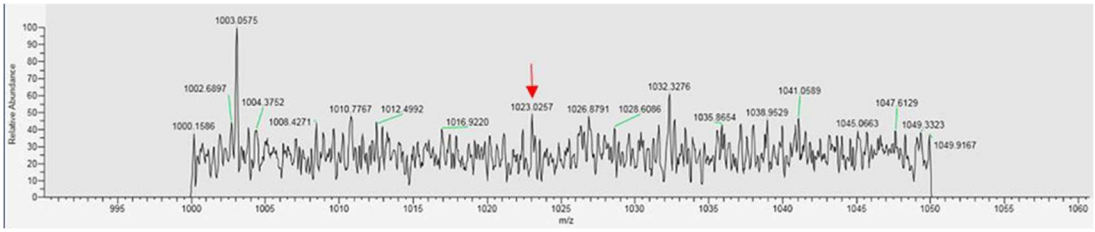

Figure 2.7: Mass spectrum of P-CTX3B in solvent solution containing MeOH/H_2O acquired in MS/MS scan mode, selected ion being *m/z* 1023.57852, collision energy at 15 eV, at 100 ppb.

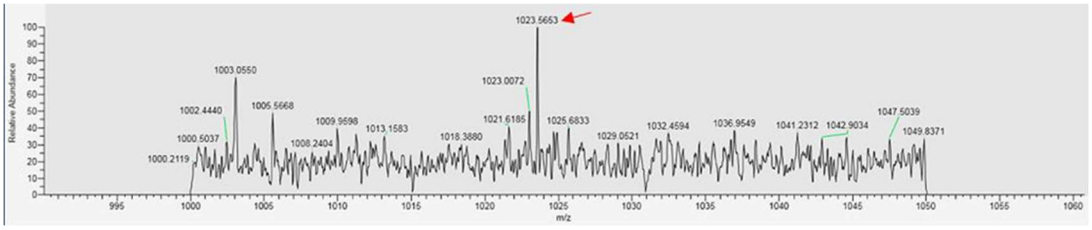

Figure 2.8: Mass spectrum of P-CTXB in solvent solution containing MeOH/H_2O acquired in positive MS/MS scan mode, selected ion being *m/z* 1023.57852, collision energy at 10 eV, at 100 ppb.

P-CTX-3C peak intensities from other studies will be used to compare with P-CTX-3B as they have the same ions. The ions that are used to categorize the MS/MS spectra of P-CTX-3C that was also described from previous studies are successive water losses at *m/z* 1005.5550 $[M- H_2O +H]^+$, *m/z* 987.5430 $[M-2H_2O+H]^+$, *m/z* 969.5311 $[M-3H_2O +H]^+$ and *m/z* 951.5311 $[M-4H_2O+H]^+$. Additionally, the opening of G-and H-rings, followed

by water losses, allowed for the formation of fragments at *m/z* 541.2880, 465.2797, 447.2616, 429.2638, and 411.2541. Finally, three different K and/or L ring fragmentations gave intense ions at *m/z* 155.1064, 125.0959 and 99.0808 (Figure 2.9).

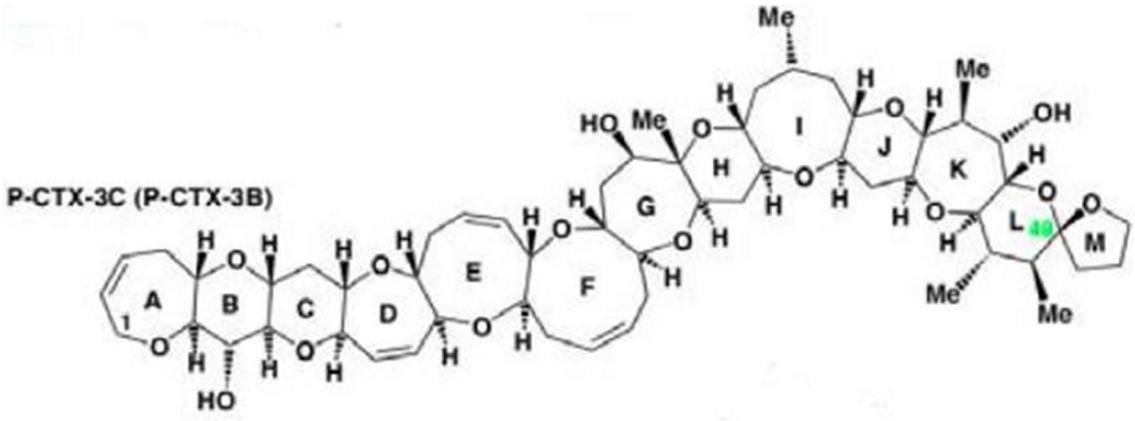

Figure 2.9: Labelled chemical structure of P-CTX-3C (P-CTX-3B) (Nicholson & Lewis, 2006).

Table 2.5 shows the 100 ppb in solvent A with 15 eV and acquired for 3 minutes. The fragmentation of the protonated ion provided the best mass which was expected as $[M+H]^+$ had the greatest peak intensity, as indicated previously. On average, the mass accuracies were still greater than 5 ppm, and the peak could not be identified with certainty. Acquiring data for a longer period could potentially improve accuracy by averaging more scans and enhancing peak determination. However, in the context of LC-MS/MS, this approach may introduce challenges such as analyte instability, degradation of system performance, and reduced sample throughput. Therefore, while longer acquisition times may offer benefits in terms of data quality, practical considerations such as system stability and sample throughput must be carefully weighed.

Table 2.5: The theoretical and measured masses (*m/z*) of P-CTX-3B most intense ion $[M+H]^{+}$. Measured masses were taken from the mass spectrum of P-CTX-3B in solvent solution containing ACN/H_2O acquired in MS/MS scan mode, selected ion *m/z* 1023.57852 collision energy at 15 eV, and concentration of 100 ppb.

Molecular Formula	Mass (Da)	Theoretical (*m/z*)	Measured (*m/z*)	Mass Accuracy (ppm)
$C_{57}H_{82}O_{16}$	1022.5603			
	$[M+H]^{+}$	1023.56756	1023.55893	-8.43
$C_{57}H_{80}O_{15}$	1004.54917	1005.55253	1005.54734	-5.16
$C_{57}H_{78}O_{14}$	986.53861	987.54196	987.53896	-3.04
$C_{57}H_{76}O_{13}$	968.5286	969.5314	969.54161	10.53
$C_{57}H_{74}O_{12}$	950.51748	951.52083	951.68502	172.53
$C_{51}H_{70}O_{14}$	906.47601	907.47936	907.46407	-16.85
$C_{31}H_{40}O_{8}$	540.27177	541.27512	541.26379	-20.93
$C_{26}H_{40}O_{7}$	464.27686	465.28021	465.34775	145.14
$C_{26}H_{38}O_{6}$	446.26629	447.26965	447.38335	254.14
$C_{26}H_{36}O_{5}$	428.25573	429.25908	429.27043	26.44
$C_{26}H_{34}O_{4}$	410.24516	411.24852	411.24153	-17.00
$C_{9}H_{14}O_{2}$	154.09883	155.10219	155.10662	28.56
$C_{8}H_{12}O$	124.08827	125.09162	125.09616	36.29

Other studies using Tandem MS with liquid chromatography applied the multiple reaction method (MRM), which is used to selectively quantify compounds within complex mixtures. Most studies that detect P-CTXs using the MRM method select the

$[M+NH_4]^+$ as the precursor ion and the ion species $[M-nH_2O+H]^+$ as the fragment ions (Lewis et al. 1998; Lewis et al. 2009; Stewart et al. 2010; Sibat et al. 2018). An alternative method was chosen in the Yogi et al. (2011) study who used MRM "transitions", focusing on the transition between the precursor and product ions ($[M+Na]^+/[M+Na]^+$), which excludes any fragmentation. The "transition" in their study refers to the fragmentation pathway taken by the precursor ion to generate the observed product ions. Represented as the m/z ratio of the precursor ion and corresponding product ion. This method only allows the identification of the CTX by comparing the retention times and mass and therefore relies on using reference standards. This method is useful for the identification of CTX but lacks specificity from the pseudo-transition $[M+Na]^+/[M+Na]^+$. In addition, it was recommended that having the precursor ion as the sodium adduct is not a preferred choice for creating MRM transition (Hopfgartner, 2017). This is because of the suppression that can be observed and the resistance to fragmentation to confirm its structure. Due to this reason, it is why selecting an ion for quantitation is important and should be tested.

2.3.5 Effect of Flow Rate

To optimize the flow rate for detecting P-CTX-3C using HRMS, various low flow rates were tested. Figure 2.10 illustrates the impact of flow rate on the peak intensity of the most intense ion of CTX3B. The standard solution, containing CTX3B at a concentration of 100 ppb in acetonitrile, was injected at flow rates of 1, 5, and 10 µL/min. All standard solutions were analyzed on the same day. The highest peak intensity, reaching 5.11E+04, was observed at 10 µL/min for the ammonium ion.

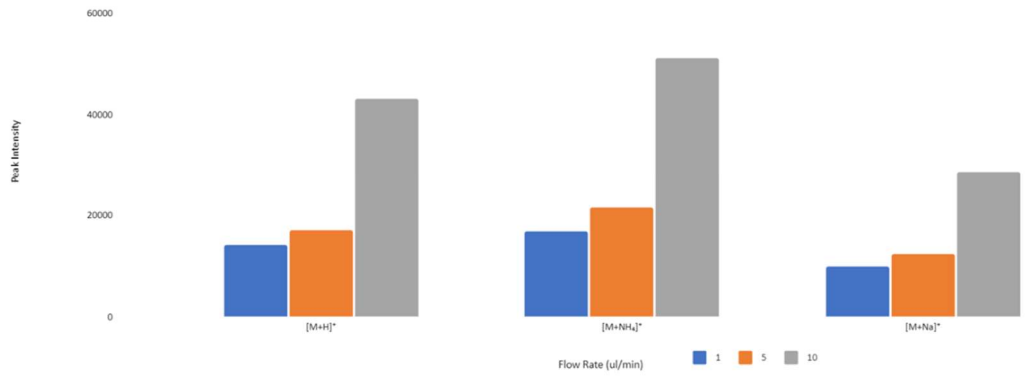

Figure 2.10: The effect of flow rate on the peak intensities using the solvent solution containing ACN/H_2O. Standard solution of P-CTX3C at 100 ppb was injected at flow rates of 1 and 5 µL/min in quadrupled (n=4, error bars = standard deviation) and 10 µL/min in triplicate (n=3, error bars = standard deviation). Selected ions monitoring were $[M+H]^+$, $[M+NH_4]^+$, and $[M+Na]^+$.

Table 2.6: Average peak intensities for P-CTX-3B, $[M+H]^{+}$, $[M+NH_4]^{+}$, and $[M+Na]^{+}$ at various flow rates, 1, 5, and 10 µL/min.

	Average		
Flow Rate (µL/min)	$[M+H]^{+}$	$[M+NH_4]^{+}$	$[M+Na]^{+}$
1	1.41E+04	1.69E+04	9.79E+03
5	1.70E+04	2.14E+04	1.22E+04
10	4.31E+04	5.11E+04	2.87E+04
Standard Deviation			
1	9.13E+03	1.18E+04	6.55E+03
5	4.59E+03	4.61E+03	3.27E+03
10	8.29E+03	9.66E+03	4.95E+03

Across all ions, it was noted that a flow rate of 10 µL/min consistently generated higher peak intensities compared to 1 µL/min and 5 µL/min. Thus, increasing the flow rate led to improved peak intensities. Sibat et al. (2018) explored the impact of flow rate during LC- MS/MS of CTXs and found that the lowest flow rate yielded greater peak intensities with acetonitrile, while the opposite was observed with methanol. They suggested that the dependence of signal response on the solvent's flow rate could be attributed to the specific design of the source interface. Further investigation into the individual solvents is necessary to determine their specific impact on the ESI source.

Hence, the ideal flow rate for high-sensitivity identification of CTXs may vary with the instruments used. Therefore, a more systematic exploration, particularly around 10 µL/min, is warranted to determine the most suitable flow rate for this method.

2.3.6 Chapter Summary

Mass accuracy was compared for P-CTX-3C ions obtained in solvent A (ACN/H_2O) and solvent B (MeOH/H_2O) solutions. Solvent B demonstrated superior accuracy for sodium adducts, while solvent A favored protonated and ammonium adducts. Analyzing a 100 ppb solution, the most intense ions $[M+H-H_2O]^+$, $[M+H]^+$, $[M+NH_4]^+$, and $[M+Na]^+$ were detectable above the LOD and LOQ, except sodium. This poses challenges for quantification of sodium at lower concentrations.

A comprehensive fragmentation study (MS2) was conducted to optimize collision energies for strong fragmentations. The protonated ion was selected for fragmentation, and varying collision energies revealed optimal fragmentation at 15 eV for solvent A, while challenges were encountered with solvent B in obtaining robust mass spectra. The greater mass accuracy for protonated ion fragments suggested improved reliability with longer acquisition times.

Lastly, different flow rates were tested, and peak intensities were observed to be highest at 10 µL/min. This underscored the significance of flow rate optimization for high-sensitivity CTX identification. The optimal flow rate depended on solvent type, aligning

with previous findings, and emphasized the need for systematic exploration to determine the most suitable flow rate for this method.

CHAPTER 3 – Identification of Ciguatoxin in Fish Sample

3.1 Introduction

This chapter includes spiked fish tissue with the CTX standard, followed by an extraction protocol for analysis using a HRMS mass spectrometer. The refined conditions established in the previous section were employed and evaluated for their effectiveness in ionization efficiency in a fish matrix. This assessment was conducted using spiked matrix- matched solutions and calibration curves, with the results discussed.

3.1.1 Extraction of CTX from Fish Tissue

Sample preparation is a fundamental part in isolating and purifying CTX from the complex matrix of fish tissue. It significantly influences the sensitivity, accuracy, and precision of CTX detection using mass spectrometry (Harwood et al., 2017). Fish ciguatoxins, being somewhat fat-soluble and present in very small concentrations, create a significant problem for identifying them chemically within the parts per billion range or lower. Thus, getting rid of the fats and other fat-soluble impurities collected alongside them is a crucial step in preparing matrix-free samples for analysis. The purification process should effectively isolate the toxins and reduce the impact of other substances that might interfere, thereby enhancing detection through bioassays and mass spectrometry methods. The methods commonly used to extract ciguatoxins from fish flesh and purify them for analysis involve several stages, such as acetone extraction,

separating them between diethyl ether and water, and removing fats using hexane. The resulting crude extract then needs further cleaning using solid phase extraction (SPE) with specific adsorbents, both normal-phase and/or reversed-phase, before it's ready for analysis (Pasinszki et al., 2020, Harwood et al., 2017, Caillaud et al., 2010, and Pottier et al., 2023). A widely employed sample preparation technique, as described in the work of Yogi et al. (2011), was further corroborated in a study conducted by Sibat et al. (2018).

The latter study employed high-resolution mass spectrometry (HRMS) for the analysis of P-CTX ciguatoxins. This selection of the analytical method was motivated by the research findings reported in Sibat et al. (2018), thereby forming the basis for the present study.

3.1.2 Importance of Matrix Effects and Calibration Curve

There are many challenges of matrix effects in mass spectrometry, especially using ESI with complex matrices and low concentrations such as ciguatoxins (Matuszewski et al., 1998, Matuszewski et al., 2003, and Kebarle & Tang, 1993). Matrix effects alter the ionization efficiency of target analytes due to co-eluting compounds, resulting in either reduced (ion suppression) or increased (ion enhancement) response, significantly impacting analytical performance. Several mechanisms of matrix effects have been observed in ESI mass spectrometry such as the alterations in surface tension of the droplets formed by electrospray. The exact mechanisms are not fully understood. However, it is generally accepted to be related to the competition for available charges and droplet surface access during electrospray analysis.

Matrix effects can influence the performance of the instrument such as HRMS. It may create false negative results due to ion suppression (Van Eeckhaut et al., 2009) or false positive results such as a signal of the internal standard (IS) undergoing suppression greater than that of the analyte (Gosetti et al., 2010). Often matrix effects cannot be avoided, only minimized. This requires optimization of sample preparation and MS conditions, which are both in focus when analyzing and detecting CTX. Enhanced sample preparation would involve measures to remove potential co-eluting compounds, cleaning the sample of impurities for analysis. Optimizing MS conditions such as the collision energies, flow rates can help improve the sensitivity for the specific analyte, reducing the background noise in the sample (Boyd et al., 2008). Matrix effects can often be mitigated through the introduction of an internal standard, typically a stable isotope surrogate of the analyte, allowing for matrix corrections. However, in this study, the absence of a suitable surrogate prevented such correction measures. Matrix effects can be quantified by calculating the matrix effect factor (MEF), which compares the peak intensity or area of an analyte in a sample with a matrix to that of the same analyte in a neat standard (without matrix). This calculation can indicate ion enhancement or suppression depending on if the MEF value is greater than one or less than one, respectively (Wang & Zhou, 2016).

A calibration curve serves as a mathematical model used to estimate the relationship between the known concentration of a substance being measured and the response observed in the measuring instrument. It helps determine the concentration of this

substance in an unknown sample (Cheng et al., 2022). Calibration curves serve as an essential tool in CTX (ciguatoxin) detection, enabling the identification of matrix effects and instrument noise. Their application in method validation aids in establishing the Limit of Detection (LOD) and Limit of Quantitation (LOQ) while also assessing matrix effects (Wu et al., 2011).

3.2 Materials and Methods

The use of extraction and a solid-phase extraction (SPE) clean-up procedure was adopted from Sibat *et al.* (2018). A total of 42 g of farmed-raised tilapia fish fillet (Latin America) was used to create our in-house test samples. The sample preparation was completed with 10 g of fish tissue that was spiked with the toxin before sample preparation (toxic sample) and 10 g of fish tissue was spiked after sample preparation (calibration sample 1) on the same day. Another set of calibration samples (calibrations sample 2) using 10 g of fish tissue was completed on a different day. Both toxic samples and calibration samples were prepared using the following procedure.

3.2.1 Standards and Chemicals

The ciguatoxin chosen for this experiment was 49-epi-CTX3C (CTX3B) provided by Dr. Mireille Chinain, Institut Louis Malardé (IRD), Tahiti, French Polynesia. The 500 µL methanol stock solution (2 ng/µL) was stored at 4°C until use.

The chemicals for the solvent solutions consisted of HPLC grade methanol, HPLC grade acetonitrile and HPLC grade ammonium, and formic acid (88% purity; Sigma-Aldrich). HPLC grade ethyl acetate and HPLC grade n-hexane (VWR Chemicals BDH) and high purity 18.2 MΩ cm^2 water produced at the Water Quality Centre, Trent University were also used.

3.2.2 Preparation of Extraction Solutions

Methanol (MeOH) solutions of (MeOH) 90%, MeOH 75%, MeOH 60%, and Ethyl acetate (EtOAc)/methanol (90/10 v/v) were created. The solutions were made in different volumes according to the amount needed for extraction: 130 mL of MeOH 90%, 20 mL of MeOH 75%, 30mL of MeOH 60%, and 100 mL of EtOAc/methanol (90/10 v/v). High purity 18.2 MΩ cm^2 water produced at the Water Quality Centre, Trent University was used to make the various MeOH solutions. The volumes of MeOH and water needed to make the solution were calculated and measured then combined and stored until use.

3.2.3 Extraction

A piece of the fish tissue was cut and weighed to approximately 10 g, minced to 1 cm pieces and extracted twice using a blender (NutriBullet® Magic Bullet Blender) with 150 mL of acetone (VWR Anachemia). The extract was divided into 4 x 50 mL falcon tubes and centrifuged (Centrifuge 5702, Eppendorf) at 3500 g for 10 min. The combined supernatants were evaporated to dryness with a rotary evaporator (Buchi, Switzerland) under reduced pressure at 60 ^{o}C in a 500 mL round bottom flask. The residue was

reconstituted in 30 mL of 90% MeOH. It was treated twice with 60 mL of n-hexane using a 125 mL separatory funnel. The top hexane layers were removed and discarded, and the aqueous methanol layers were combined and put under the rotary evaporator under reduced pressure at 60 ^{o}C. The crude extract was dissolved in 5 mL EtOAc/methanol (90/10, v/v) before purification, using two successive SPE cleanup steps.

3.2.4 SPE-Clean up

Florisil SPE cartridges (Silicycle, SiliaPrep, 500 mg) were first conditioned with 3 mL of EtOAc/methanol (90/10, v/v), prior to loading the sample extracts (2 mL). Cartridges were eluted twice with 2 mL of the same solvent. The three fractions were combined (6 mL) and evaporated under N_2 gas using a nitrogen evaporator (N-evap) (Organomation). The purified extract was dissolved in MeOH 60% (2 mL).

For the second SPE purification, a SPE vacuum manifold (Supelco Visiprep 24, Fisher Scientific) was used to hold the cartridges and aid the elution of the samples. The cartridges 60A C18 (17%) (Silicycle, SiliaPrep, 500mg) were first conditioned with 3 mL of 60% MeOH. The purified extract was loaded into the cartridges. The C18 cartridges were washed with 3 mL 75% MeOH and the P-CTXs were eluted twice with 3 mL of 90% aqueous MeOH. The two eluting fractions were combined (12 mL) and evaporated under N_2 gas using an N-evap. The purified extract was reconstituted with 500 µL of MeOH before analysis.

3.2.5 Sample Preparation of Calibration Samples

The purified blank fish sample (500 µL) was separated into 5 solutions (each 100 µL). Four of the solutions were spiked with the toxin at concentrations of 10, 20, 50, and 100 ppb (Eqn. 1 provides an example calculation of the volume required to obtain a concentration of 10 ppb). The samples were stored and chilled (4 °C) until analysis.

$$\text{Eqn. 1: } 2000 \text{ ppb} * (V1) = 10 \text{ ppb} * (100 \text{ µL}) \quad V1 = 0.5 \text{ µL}$$

The concentration of CTX-3B in fish tissue for the calibration solutions are 5 ng, 10 ng, 25 ng, and 50 ng per gram of fish tissue respectively.

3.2.6 Sample Preparation of Spiked Fish Sample

A purified 1000 µL toxic fish sample was created by spiking the fish before sample preparation. The 10 g of fish was spiked with 50 µL of the toxin and left to rest for 30 minutes, allowing the toxin to permeate into the tissue prior to extraction. The concentration of CTX-3B in the final sample is 100 ppb. The concentration of CTX-3B in the final sample is 10 ng per gram of fish tissue. The sample was stored and chilled (4°C) until analysis.

3.2.7 HRMS analysis of Calibration and Spiked Fish Samples

For both calibration solutions 1 (prepared same day as the spiked fish sample) and 2 (prepared on a separate day), the blank solution from the samples was introduced to the

Thermo Scientific QExactive Orbitrap directly via a 250 µL syringe (SGC Engineering, Fisher Scientific) before the samples were analyzed. The samples with concentrations of 10, 20, 50, and 100 ppb were analyzed respectively, and 3 replicates of the mass spectra were acquired. Mass spectrometric detection was performed using full scan mode with a flow rate of 5 µL/min and acquired for 30 seconds, due to the limited amount of solution. The blank solution from calibration solutions was introduced to the Orbitrap directly via a 250 µL syringe and acquired before the sample was analyzed. The sample and calibration solutions were analyzed under full scan mode with a flow rate of 5 µL/min and acquired for 1 minute. The sample was additionally acquired in MS2 mode, where the precursor ions $[M+H]^+$, $[M+Na]^+$ and $[M+NH_4]^+$were fragmented to obtain their respective product ions. This analysis was conducted at a flow rate of 5 µL/min, with a normalized collision energy (NCE) of 15 eV, and data acquisition was performed for a duration of 3 minutes.

3.2.8 Matrix Effect Factor (MEF)

The Matrix Effect Factor (MEF) was calculated according to Equation 2:

Eqn. 2: MEF= (Response in Sample Matrix)/(Response in Standard solution)

Where:

- "Response in Sample Matrix" refers to the peak intensity or area of the analyte in the sample with the matrix
- "Response in Standard solution" is the peak intensity or area of the analyte in a standard solution without the matrix

- MEF > 1: A value greater than 1 indicates signal enhancement, meaning the matrix increases the response of the analyte. This can happen if the matrix improves analyte ionization or stability.
- MEF < 1: A value less than 1 indicates signal suppression, meaning the matrix decreases the response of the analyte. This can occur if the matrix interferes with analyte ionization, causes ion suppression, or affects the detector response.
- MEF = 1: A value of 1 implies no matrix effect; the matrix has no impact on the analyte signal.

3.3 Results/Discussion

3.3.1 Solvent Chemistry

Figure 3.1 compares the full scan mass spectrum of the CTX standard in solution with solvent A with the full scan mass spectrum of the fish sample spiked with CTX. Table 3.1 lists the ion intensities for the most intense peaks in the spiked fish sample mass spectrum and their mass accuracies. The ion with the most intense peak in the spiked fish sample was the sodium adduct observed at *m/z* 1045.62241 $[M+Na]^+$ with ion intensity of 1.02E+06. The next most intense peak was the protonated molecule *m/z* 1023.64734 $[M+H]^+$ with ion intensity of 8.41E+05. This is followed by the $[M+H-H_2O]^+$ with ion intensity of 3.96E+05. Lastly the ammonium ion $[M+NH_4]^+$ *m/z* 1040.68777 was the least intense peak with ion intensity of 3.81E+05.The spiked fish sample mass spectrum was observed to have the opposite order of intensities compared to the CTX standard sample spectrum where the sodium ion was the least abundant and the protonated ion being the most abundant out of the CTX related ions. This aligned with other literature as

the protonated and sodium adducts were most often the most abundant peaks in fish tissue samples (Murray et al., 2018). The lowest abundant peak was the sodium adduct when the standard was just in the standard solution containing acetonitrile. However, the sodium adduct was the most intense CTX peak from the toxic fish sample. The sodium adducts peak intensity could be due to the great stability of the sodium adduct in fish tissue as noted previously (Sibat et al., 2018).

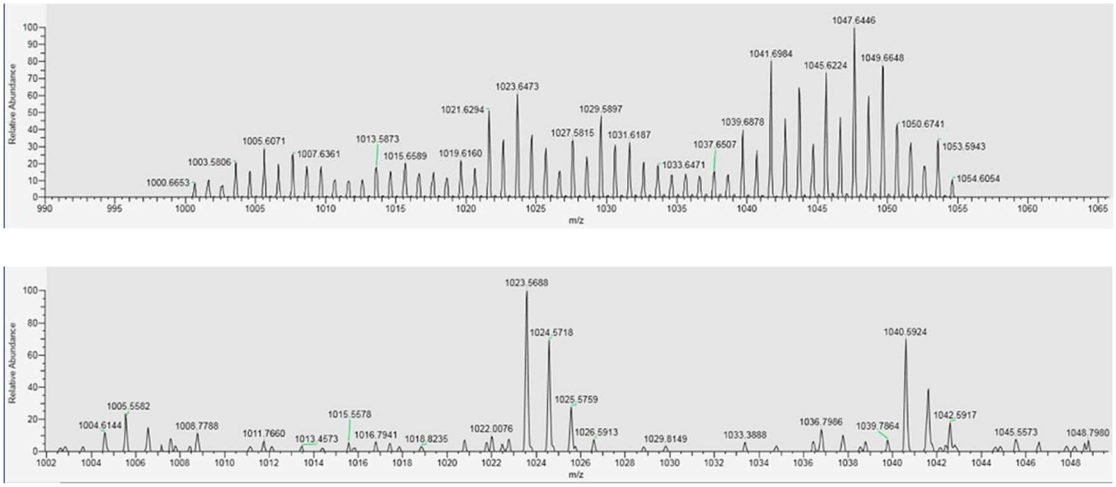

Figure 3.1: Comparison between full scan spectrum of toxic fish sample (top) and full scan spectrum of P-CTX3B toxin in solvent solution containing ACN/H_2O (bottom).

Table 3.1: The theoretical and measured masses (*m/z*) of P-CTX-3B $[M+H-H_2O]^+$, $[M+H]^+$, $[M+NH_4]^+$, and $[M+Na]^+$. Measured masses and peak height were taken from the mass spectrum of the toxic fish sample in full scan mode (Figure 3.1). The mass accuracies were calculated from the theoretical and measured peaks.

Ions	**Theoretical (*m/z*)**	**Measured (*m/z*)**	**Mass Accuracy (ppm)**	**Peak height**
$[M+H-H_2O]^+$	1005.55253	1005.60709	54.26	3.96E+05
	1006.55588	1006.61427	58.01	2.69E+05
$[M+H]^+$	1023.56756	1023.64734	77.94	8.41E+05
	1024.57092	1024.65356	80.65	5.09E+05
	1025.57427	1025.67134	94.64	1.39E+06
	1026.57763	1026.64751	68.07	1.39E+06
	1027.57852	1027.58148	2.88	4.65E+05
$[M+NH_4]^+$	1040.59411	1040.68777	90.00	3.81E+05
	1041.59747	1041.69836	96.85	1.11E+06
	1042.60082	1042.70803	102.82	6.41E+05
	1043.60418	1043.72086	111.79	1.39E+06
	1044.60570	1044.69838	88.71	4.34E+05
$[M+Na]^+$	1045.54951	1045.62241	69.72	1.02E+06
	1046.55286	1046.62808	71.87	1.39E+06

3.3.2 Mass Accuracy and Matrix effect

Table 3.1 lists the mass accuracy and peak height of the most intense ions of P-CTX from the full scan mass spectrum of the toxic fish sample. The mass accuracies for the spiked fish sample all have decreased compared to analyzing the CTX standard solution and were generally poor (> 5 ppm). This suggests that the P-CTX-3B ions in the toxic fish sample cannot be identified with great confidence. The poor mass accuracies were anticipated due to the complexity of the fish matrices that can provide more interferences. However, the peak intensities for the ions in the spiked fish sample was greater than those from the CTX standard solutions.

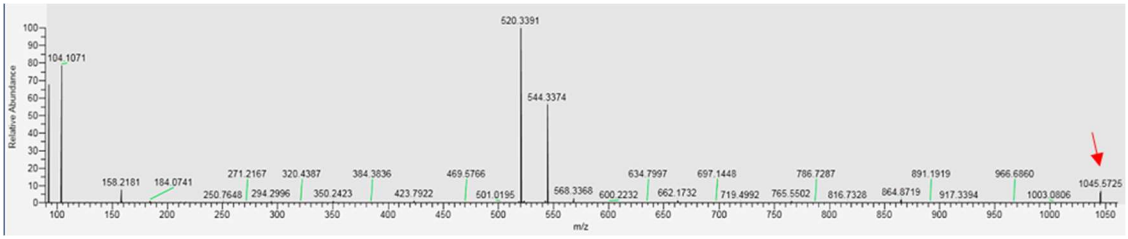

Figure 3.2: Mass spectrum of toxic fish sample acquired in positive MS/MS scan mode, selected ion *m/z* 1045.54951, collision energy at 15 eV.

Table 3.2: The theoretical masses (Da) and measured masses of P-CTX-3B most intense ions $[M+H-H_2O]^+$, $[M+H]^+$, $[M+NH_4]^+$, and $[M+Na]^+$. Measured masses were taken from the mass spectrum of the toxic fish sample in MS/MS scan mode with $[M+Na]^+$ as the selected ion (Figure 3.2). The mass accuracies were calculated from the theoretical and measured peaks.

Molecular Formula	**Mass (Da)**	**Theoretical (*m/z*)**	**Measured (*m/z*)**	**Mass Accuracy (ppm)**
$C_{57}H_{82}O_{16}$	1022.5603			
$[M + NH_4]^+$				
$[M+H]^+$				
	$[M + Na]^+$	1045.54951	1045.572478	21.97
$C_{57}H_{80}O_{15}$	1004.54917	1005.55253	1005.36969	-181.86
$C_{57}H_{78}O_{14}$	986.53861	987.54196	987.40023	-143.54
$C_{57}H_{76}O_{13}$	968.52860	969.53140	969.40419	-131.22
$C_{57}H_{74}O_{12}$	950.51748	951.52083	951.5346	14.47
$C_{51}H_{70}O_{14}$	906.47601	907.47936	907.7374	284.27
$C_{31}H_{40}O_8$	540.27177	541.27512	541.32364	89.63
$C_{26}H_{40}O_7$	464.27686	465.28021	465.17776	-220.24
$C_{26}H_{38}O_6$	446.26629	447.26965	446.28246	-2212.03
$C_{26}H_{36}O_5$	428.25573	429.25908	429.26258	8.15
$C_{26}H_{34}O_4$	410.24516	411.24852	411.26389	37.37
$C_9H_{14}O_2$	154.09883	155.10219	155.10819	38.68
$C_8H_{12}O$	124.08827	125.09162	125.08628	-42.69
$C_6H_{10}O$	98.07262	99.07597	99.06065	-154.65

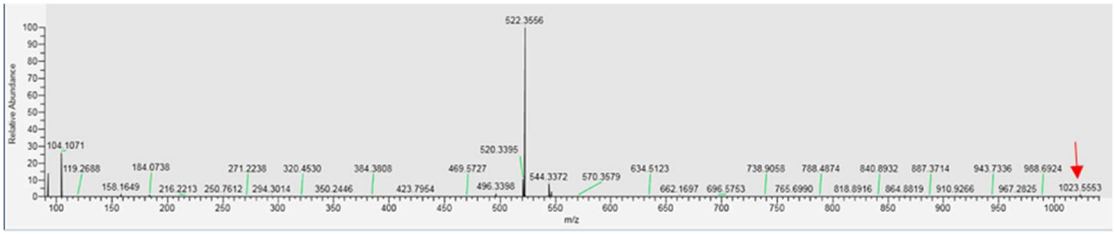

Figure 3.3: Mass spectrum of toxic fish sample acquired in positive MS/MS scan mode, selected ion *m/z* 1023.56756, collision energy at 15 eV.

Table 3.3: The theoretical masses (Da) and measured masses of P-CTX-3B most intense ions $[M+H-H_2O]^+$, $[M+H]^+$, $[M+NH_4]^+$, and $[M+Na]^+$. Measured masses were taken from the mass spectrum of the toxic fish sample in MS/MS scan mode with $[M+H]^+$ as the selected ion (Figure 3.3). The mass accuracies were calculated from the theoretical and measured peaks.

Molecular Formula	**Mass (Da)**	**Theoretical (*m/z*)**	**Measured (*m/z*)**	**Mass Accuracy (ppm)**
$C_{57}H_{82}O_{16}$	1022.5603			
$[M + NH_4]^+$				
	$[M+H]^+$	1023.56756	1023.55527	-12.01
$[M + Na]^+$				
$C_{57}H_{80}O_{15}$	1004.54917	1005.55253	1005.17454	-376.04
$C_{57}H_{78}O_{14}$	986.53861	987.54196	987.51229	-30.05
$C_{57}H_{76}O_{13}$	968.52860	969.53140	969.69469	168.39
$C_{57}H_{74}O_{12}$	950.51748	951.52083	951.53564	15.56
$C_{51}H_{70}O_{14}$	906.47601	907.47936	907.47113	-9.07
$C_{31}H_{40}O_8$	540.27177	541.27512	541.39385	219.30
$C_{26}H_{40}O_7$	464.27686	465.28021	465.26892	-24.27
$C_{26}H_{38}O_6$	446.26629	447.26965	447.22459	-100.75
$C_{26}H_{36}O_5$	428.25573	429.25908	429.22459	-80.35
$C_{26}H_{34}O_4$	410.24516	411.24852	411.1958	-128.21
$C_9H_{14}O_2$	154.09883	155.10219	155.09771	-28.89
$C_8H_{12}O$	124.08827	125.09162	125.84111	5955.84
$C_6H_{10}O$	98.07262	99.07597	99.075219	-7.58

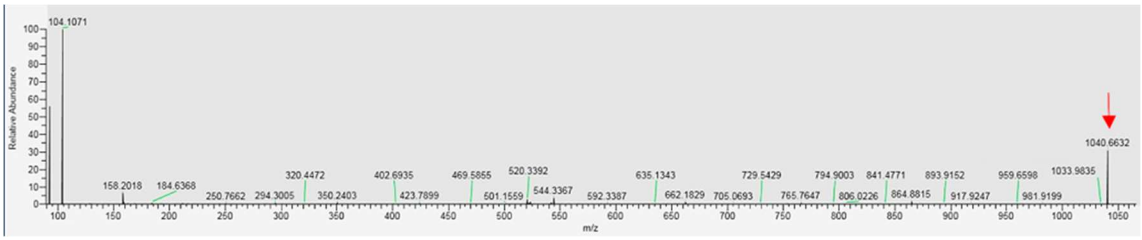

Figure 3.4: Mass spectrum of toxic fish sample acquired in positive MS/MS scan mode, selected ion *m/z* 1040.68777, collision energy at 15 eV.

Table 3.4: The theoretical masses (Da) and measured masses of P-CTX-3B most intense ions $[M+H-H_2O]^+$, $[M+H]^+$, $[M+NH_4]^+$, and $[M+Na]^+$. Measured masses were taken from the mass spectrum of the toxic fish sample in MS/MS scan mode with $[M+NH_4]^+$ as the selected ion (Figure 3.4). The mass accuracies were calculated from the theoretical and measured peaks.

Molecular Formula	Mass (Da)	Theoretical (*m/z*)	Measured (*m/z*)	Mass Accuracy (ppm)
$C_{57}H_{82}O_{16}$	1022.5603			
	$[M + NH_4]^+$	1040.59411	1040.663181	66.37
$[M+H]^+$				
$[M + Na]^+$				
$C_{57}H_{80}O_{15}$	1004.54917	1005.55253	1005.571168	18.53
$C_{57}H_{78}O_{14}$	986.53861	987.54196	987.48714	-55.51
$C_{57}H_{76}O_{13}$	968.5286	969.5314	969.65686	129.39
$C_{57}H_{74}O_{12}$	950.51748	951.52083	951.6459	131.42
$C_{51}H_{70}O_{14}$	906.47601	907.47936	907.49805	20.60
$C_{31}H_{40}O_8$	540.27177	541.27512	541.15001	-231.19
$C_{26}H_{40}O_7$	464.27686	465.28021	465.35555	161.90
$C_{26}H_{38}O_6$	446.26629	447.26965	447.22308	-104.13
$C_{26}H_{36}O_5$	428.25573	429.25908	429.15234	-248.72
$C_{26}H_{34}O_4$	410.24516	411.24852	411.2943	111.31
$C_9H_{14}O_2$	154.09883	155.10219	155.10369	9.67
$C_8H_{12}O$	124.08827	125.09162	125.09387	17.99
$C_6H_{10}O$	98.07262	99.07597	99.06118	-149.30

Matrix interference, causing either ion enhancement or suppression, is a common issue in ESI-MS analysis. When detecting CTXs by ESI-MS, matrix effects are most likely present and was assumed to relate to the remaining fish oil content in the analyzed sample. Matrix effects can significantly impact the accuracy and reliability of the analysis and therefore needs to be considered when detecting P-CTXs (Lewis et al., 2009). To determine matrix inference in the spiked fish tissue sample, the MEF was calculated for the most intense ions of P-CTX. All the adducts had a MEF > 1 indicating ion enhancement has taken place, a phenomenon where the matrix increases the response of the analyte. This can happen if the matrix improves analyte ionization or stability (Wu et al., 2011). The opposite matrix effect was also observed. For example, a previous study concluded ion suppression from their fish matrices specifically the sodium ion. As a result, a fish matrix of red snapper suppressed the intensity of the sodium ion versus the ion's intensity when the standard was just dissolved in methanol (Murray et al., 2018). The ions that were the least affected by matrix effects were the ammonium ion (MEF = 7.02) and the protonated ion (MEF = 10.42) which suggests that ammonium and protonated ions may be more reliable for monitoring as they are the least affected by changes in the matrix compared to other ions. This reflects previous literature where the detection of P-CTX-1 and P-CTX-3C using ESI-triple quadrupole/linear ion traps had better selectivity, sensitivity with less matrix effects when choosing the ammonium and protonated ions as precursors (Sibat et al., 2018).

3.3.3 Fragmentation study (MS2)

Figure 3.2, 3.3, and 3.4 are the MS2 scan mass spectra of the CTX spiked fish sample with NCE value of 15 eV for each of the product ions generated from the most intense precursor ions *m/z* 1045.54951 $[M+Na]^+$ *, m/z* 1023.56756 $[M+H]^+$, and *m/z* 1040.59411 $[M+NH_4]^+$, respectively.

P-CTX-3C peak *m/z* ratios from other studies will be used to compare with P-CTX-3B as they generate the same ions. The ions that are used to categorize the MS/MS spectra of P-CTX-3C that was also described from previous studies are successive water losses at *m/z* 1005.5550 $[M- H_2O+H]^+$, *m/z* 987.5430 $[M-2H_2O+H]^+$, *m/z* 969.5311 $[M-3H_2O +H]^+$ and *m/z* 951.5311 $[M-4H_2O+H]^+$. Additionally, the opening of G-and H-rings, followed by water losses, allowed for the formation of protonated ion fragments at *m/z* 541.2880, on one hand, and *m/z* 465.2797, 447.2616, 429.2638, 411.2541, on the other hand. Finally, three different K and/or L ring fragmentations gave intense product ions at *m/z* 155.1064, 125.0959 and 99.0808 (Figure 2.9). The mass accuracies for each of the ions were poor a (> 5 ppm) therefore these ions cannot be identified coming from P-CTX-3B with strong confidence.

Even though the sodium ion was the most intense peak in the spiked fish sample during full scan analysis, the peak with the best mass accuracy from the fragmentation mass spectra came from the fragmentation of the protonated ion (12 ppm). The ammonium ion was observed to have the poorest mass accuracy values (> 5 ppm) and was the least abundant ion out of the three ions in the full scan spiked fish sample mass spectrum.

Most of the fragmented ions contributed to poor mass accuracies (> 5 ppm) and therefore are less confidently identified as being part of P-CTX-3B. The fragmentation of both sodium and protonated ions exhibited a peak with m/z values of 522.3556 and 520.3391, respectively, each at 100% intensity. However, based on previous literature regarding product ions for P-CTX-3C/B, there is no indication of ions corresponding to these specific m/z values. The ion at *m/z* 522.3556 may be associated with the fragment derived from the previously investigated compound $C_{31}H_{40}O_8$ at *m/z* 540.2723, with the subtraction of H_2O resulting in the observed fragment $C_{31}H_{38}O_7$. Notably, this fragment has not been observed with high intensities in earlier studies. Similarly, the ion at *m/z* 520.3391 may be linked to the removal of 2H from $C_{31}H_{38}O_7$, forming the fragment $C_{31}H_{36}O_7$, which has also not been observed at such intensity in previous research. An alternative explanation could involve the fragmentation of an ion either below or above the precursor ion's mass, influenced by the fragmentation window spanning *m/z* 0.2.

3.3.4 Limit of Detection (LOD) and Limit of Quantitation (LOQ)

Table 3.8 presents the limit of detection and limit of quantitation for P-CTX-3B ions in the blank matrix solution. In Table 3.9, a comparison is made between the peak heights of P-CTX-3B ions in the spiked solutions and the limits of detection (LOD) and quantitation (LOQ) in a blank solution containing acetonitrile. The peak heights of each ion were assessed against the LOD to evaluate the method's reliability, determining whether the peaks significantly differ from the blank signal.

Table 3.8: Average, standard deviation, limit of detection and limit of quantitation of P-CTX-3B ions in the blank matrix solution.

Blank	**Peak Height**			
	$[M+H-H_2O]^+$	$[M+H]^+$	$[M+NH_4]^+$	$[M+Na]^+$
Run 1	3.15E+05	2.80E+05	3.07E+05	5.29E+05
Run 2	3.48E+05	3.39E+05	3.73E+05	6.24E+05
Run 3	3.92E+05	3.77E+05	4.08E+05	6.85E+05
Average	3.52E+05	3.32E+05	3.63E+05	6.13E+05
SD	38630.73	48877.398	51286.775	78615.096
LOD	4.68E+05	4.79E+05	5.17E+05	8.49E+05
LOQ	7.38E+05	8.21E+05	8.76E+05	1.40E+06

Table 3.9: Comparison of P-CTX-3B ions peak height (spiked fish sample) with the limit of detection and limit of quantitation of the blank.

Ions	**Peak height**	**LOD**	**LOQ**
$[M+H-H_2O]^+$	3.96E+05	< LOD	< LOQ
$[M+H]^+$	8.41E+05	> LOD	> LOQ
$[M+NH_4]^+$	3.81E+05	< LOD	< LOQ
$[M+Na]^+$	1.02E+06	> LOD	< LOQ

Contrastingly, the primary ions $[M^{+}H]^{+}$ and $[M+Na]^{+}$ were both found to be above the LOD and, therefore, identifiable from the blank. However, the ions $[M+H-H_2O]^{+}$ and $[M+NH_4]^{+}$ were all below the LOD, making confident identification unattainable. All ions were found below the LOQ, except the protonated ion. Consequently, confidently attributing the observed peak at this concentration becomes more challenging.

3.3.5 Calibration Curve

The calibration solutions for the most intense ions at each concentration were found to be below the limit of detection (LOD). The peak intensities did not exceed the instrument's noise level sufficiently to facilitate a proper calibration analysis. Notably, the calibration solutions at each concentration exhibited similar responses, resulting in a more linear slope (Figure 3.5). An anticipated increase in peak intensity with rising toxin concentration, from matrix effects, was not observed as expected.

One ion that exhibited a positive and linear response was $[M+H-H_2O]^{+}$ when concentration samples of 10, 20, and 50 ppb were plotted, yielding an R^2=0.9619 ($p>0.05$). Following sample preparation and solid-phase extraction (SPE), a calibration curve was constructed for fish samples spiked with 10, 20, and 50 ppb of P-CTX3C standard. Figure 2.9 illustrates the relationship between the peak intensity of $[M+H-H_2O]^{+}$ and the concentration of P-CTX-3B. The blue line represents the calibration curve derived from the fish sample, while the orange curve depicts the calibration curve of the standard P-CTX-3C in an ACN/H_2O solution, utilizing the peak intensity of $[M+H-H_2O]^{+}$. The calibration curve demonstrated ion enhancement, as evidenced by the curve

of the fish samples (blue) falling above the standard solution (orange). A study comparing the slope of the matrix-matched calibration curve to that of the curve constructed with standards in pure methanol revealed a reduction in the response of P-CTX-1, indicative of ion suppression. This phenomenon was attributed to the presence of lipids in the extract, increasing background noise (Wu et al., 2011). It is notable that the observed ion enhancement might be specific to P-CTX3B of interest, or numerous factors, including the addition of sodium in solvents, could contribute to this effect. Additionally, we were limited in solvent availability for the standard solution, resulting in insufficient data to accurately depict the curve.

However, based on the limit of detection for this response, the ion was not detected above the noise level, limiting the confidence in making conclusions (Table 3.10).

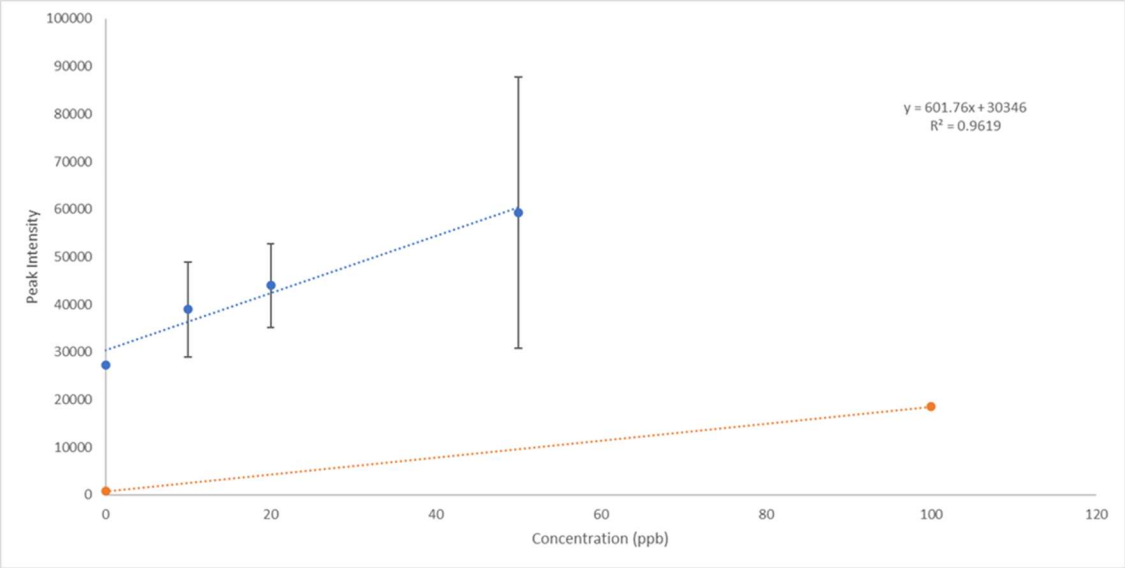

Figure 3.5: Calibration curve of fish sample spiked with 10, 20, and 50 ppb of P-CTX3C standard after sample preparation and SPE. Peak intensity of *m/z* $[M+H-H_2O]^+$ versus the concentration of P-CTX-3B (Blue). P-CTX-3C in acetonitrile solution using the peak intensity of the *m/z* $[M+H-H_2O]^+$ (Orange).

Table 3.10: Comparison of P-CTX-3B ions peak height (calibration sample made a different day from the spiked fish sample) with the limit of detection and limit of quantitation of the blank.

CTX-3B solution (ppb)	**Average peak height of $[M+H-H_2O]^+$**	**Standard Deviation**	**LOD**
10	3.90E+04	9.95E+03	< LOD
20	4.40E+04	8.76E+03	< LOD
50	5.43E+04	2.85E+04	< LOD

In LC-MS/MS analysis, it is desirable to use isotopically labeled internal standards to overcome the instrument's changing sensitivity to different matrices. Unfortunately, the absence of commercially available isotopically labeled P-CTX standards led researchers to explore alternative internal standards such as brevetoxin. However, the differential retention time and matrix effects responses differed from those of the analyte, making chemicals like brevetoxin less ideal internal standards for CTX detection (Lewis et al., 1998).

The purpose of using an internal standard is to correct for analyte loss during sample preparation or sample inlet and to mitigate matrix effects in LC-MS/MS analysis. In P-CTX analysis, QA/QC procedures like matrix spike recovery are employed in each batch to assess P-CTX recovery during sample preparation. The construction of a matrix-matched calibration curve helps minimize and improve phenomena like ion suppression or enhancement through dilution (Wu et al., 2011). Unfortunately, an internal standard was unavailable for this study.

3.3.6 Chapter Summary

The comparison of full scan mass spectra obtained from CTX standard solution, and the spiked fish sample reveals variations in ion intensities, with the order of intensities differing between the two. The sodium adducts prominence in the fish sample is attributed to its stability in fish tissue, aligning with existing literature findings. Mass accuracy and matrix effects are explored, indicating a decrease in mass accuracies for P-CTX-3B ions in the fish sample compared to the CTX standard, posing challenges for

confident identification. Matrix Effect Factors (MEFs) highlight ion enhancement in the fish sample, with protonated molecules and ammonium adducts exhibiting greater resistance to matrix effects. Fragmentation studies reveal poor mass accuracies affecting identification confidence and suggests an inverse relationship between peak intensities and mass accuracies. The determination of limits of detection and quantitation underscores challenges, with certain ions falling below the LOD and LOQ. Calibration curve complexities are discussed, emphasizing the impact of matrix effects on responses. Despite encountered challenges, a positive and linear response is observed for $[M+H-H_2O]^+$. The presence of ion enhancement in the fish sample compared to the standard prompts consideration of various factors, including matrix composition and sodium addition. Challenges were met when confidently detecting and quantifying P-CTX-3B in fish samples using mass spectrometry. It is important to account for various factors to enhance the reliability of CTX analysis in fish samples. Incorporating appropriate internal standards would further enhance the identification and quantitation of the target analyte, ensuring more accurate and precise results.

CHAPTER 4: Overall Conclusion and Future Research and Recommendations for CTX Detection

Detecting ciguatoxins (CTXs) in biological samples is challenging due to their low concentrations, various congeners, limited availability of standards, matrix interferences in fish tissue, and the unpredictable occurrence of CTX incidents. Unlike many other marine biotoxins, there is no standardized method for CTX detection. The commonly

used LC-MS/MS method provides adequate sensitivity, but suggestions have been made for using LC-HRMS with a reference standard for the most accurate CTX identification (Sibat et al., 2018).

This study aims to enhance the understanding and detection methodologies of CTX in biological materials. Employing HRMS using a reference standard, it was identified that the protonated molecules ($[M+H]^+$) were most abundant, with solvent A showing superior sensitivity. It was observed that at a concentration of 100 ppb, CTX signals were above the limit of detection (LOD) and limit of quantitation (LOQ) with the exception of the sodium ion.

Fragmentation studies stress the importance of collision energy optimization, particularly at 15 eV for protonated ions. Flow rate optimization at 10 µL/min enhances peak intensities, underscoring the significance of flow rate in high-sensitivity CTX identification. It is recommended to consider ACN/H_2O as the primary solvent for this specific HRMS method, as it offers the highest sensitivity, a perspective not widely discussed in existing literature.

Additionally, challenges were met when detecting CTX-3B in the fish tissue samples. The variation of ion peak intensities between the standard and sample solution, and matrix effects of ion enhancement for the spiked fish sample suggests the need to further explore the understanding of matrix influence on the detection of CTX. Clearly, future research should involve identifying and developing a reliable internal standard for CTX

detection, aiming to mitigate the substantial impact of complex matrices on CTX, where these toxins are naturally found. Additionally, the ongoing pursuit of a method that is rapid, simple, and sensitive remains a significant challenge for future research. This study stands out for its particular emphasis on the P-CTX-3B analogue, offering specific parameter options that improve the ion efficiency of P-CTX-3B ions. This contribution is valuable for advancing the development of a more precise methodology for analyzing this specific congener.

Overall, the study serves as a foundational step in comprehending and detecting CTX, emphasizing the continuous necessity for re-evaluation and testing of methodologies. It contributes to the broader goal of establishing a more clarified and rugged method for identifying CTX in fish. Despite significant advances, the study acknowledges the absence of an ideal assay, outlining the key challenges for future research in the field of ciguatera detection.

References

U.S. Department of Health and Human Services Food and Drug Administration Center for Food Safety and Applied Nutrition (2020). *Fish and Fishery Products Hazards and Controls Guidance, Fourth Edition*. Washington, D.C., USA https://www.fda.gov/media/80637/download

Acosta, F. (2015). Ciguatera, an emerging human poisoning in Europe. *Journal of Aquaculture & Marine Biology*, *3*(1). https://doi.org/10.15406/jamb.2015.03.00053

Alexander, J., Ceccatelli, S., Boobis, A., & Benford, D. (2010). Scientific opinion on marine biotoxins in shellfish – emerging toxins: Ciguatoxin Group. *EFSA Journal, 8*(6), 1-38 . https://doi.org/10.2903/j.efsa.2010.1627

Ansdell, V. (2019). Seafood poisoning. *Travel Medicine*, *4*, 449–456. https://doi.org/10.1016/b978-0-323-54696-6.00049-5

Armbruster, D., & Pry, T. (2008). Limit of Blank, Limit of Detection and Limit of Quantitation. *Clin Biochem Rev, 29*, 49-52

Benoit, E., Meunier, F. A., Ouanounou, G., Suput, D., & Molgo, J. (1997). Ionic basis of the nodal swelling induced by the sea anemone toxin, equinatoxin-II, in myelinated axons. *Toxicon*, *35*(12), 1661. https://doi.org/10.1016/s0041-0101(97)90085-4

Bottein, M.-Y. D., Kashinsky, L., Wang, Z., Littnan, C., & Ramsdell, J. S. (2011). Identification of ciguatoxins in Hawaiian monk seals *Monachus schauinslandi* from the northwestern and Main Hawaiian Islands. *Environmental Science & Technology*, *45*(12), 5403–5409. https://doi.org/10.1021/es2002887

Boyd, R. K., Basic, C., & Bethem, R. A. (2008). Trace Quantitative Analysis by Mass Spectrometry. *Wiley: Chichester,* https://doi.org/10.1002/9780470727140

Brenton, A. G., & Godfrey, A. R. (2010). Accurate mass measurement: Terminology and treatment of Data. *Journal of the American Society for Mass Spectrometry*, *21*(11), 1821–1835. https://doi.org/10.1016/j.jasms.2010.06.006

Caillaud, A., De la Iglesia, P., Darius, H. T., Pauillac, S., Aligizaki, K., Fraga, S., Chinain, M., & Diogène, J. (2010). Update on methodologies available for Ciguatoxin Determination: Perspectives to confront the onset of Ciguatera fish poisoning in Europe. *Marine Drugs*, *8*(6), 1838–1907. https://doi.org/10.3390/md8061838

Cameron, J., Flowers, A. E., & Capra, M. F. (1991a). Effects of ciguatoxin on nerve excitability in rats (part I). *Journal of the Neurological Sciences*, *101*(1), 87–92. https://doi.org/10.1016/0022-510x(91)90021-x

Cameron, J., Flowers, A. E., & Capra, M. F. (1991b). Electrophysiological Studies on Ciguatera poisoning in man (part II). *Journal of the Neurological Sciences*, *101*(1), 93–97. https://doi.org/10.1016/0022-510x(91)90022-y

Cheng, W. L., Markus, C., Lim, C. Y., Tan, R. Z., Sethi, S. K., & Loh, T. P. (2022). Calibration practices in clinical mass spectrometry: Review and recommendations. *Annals of Laboratory Medicine*, *43*(1), 5–18. https://doi.org/10.3343/alm.2023.43.1.5

Chinain, M., Gatti, C. M. i., Darius, H. T., Quod, J.-P., & Tester, P. A. (2021). Ciguatera poisonings: A global review of occurrences and trends. *Harmful Algae*, *102*, 101873. https://doi.org/10.1016/j.hal.2020.101873

Chinain, M., Gatti, C. M., Roué, M., & Darius, H. T. (2019). Ciguatera poisoning in French Polynesia: Insights into the novel trends of an ancient disease. *New Microbes and New Infections*, *31*, 100565. https://doi.org/10.1016/j.nmni.2019.100565

Chinain, Mireille, Darius, H. T., Ung, A., Fouc, M. T., Revel, T., Cruchet, P., Pauillac, S., & Laurent, D. (2010). Ciguatera Risk Management in French Polynesia: The case study of raivavae island (Australes Archipelago). *Toxicon*, *56*(5), 674–690. https://doi.org/10.1016/j.toxicon.2009.05.032

Codrean, S., Kruit, B., Meekel, N., Vughs, D., & Béen, F. (2023). Predicting the diagnostic information of tandem mass spectra of environmentally relevant compounds using machine learning. *Analytical Chemistry*, *95*(42), 15810-15817 https://doi.org/10.1021/acs.analchem.3c03470

Colman, J. R., Dechraoui, M.-Y. B., Dickey, R. W., & Ramsdell, J. S. (2004).

Characterization of the developmental toxicity of Caribbean ciguatoxins in finfish embryos. *Toxicon*, *44*(1), 59–66. https://doi.org/10.1016/j.toxicon.2004.04.007

Costa, P. R., Lage, S., Barata, M., & Pousão-Ferreira, P. (2011). Uptake, transformation, and elimination kinetics of paralytic shellfish toxins in white seabream (diplodus sargus). *Marine Biology*, *158*(12), 2805–2811. https://doi.org/10.1007/s00227-011-1779-3

Dechraoui Bottein, M.-Y., Wang, Z., & Ramsdell, J. S. (2011). Toxicokinetics of the ciguatoxin P-ctx-1 in rats after intraperitoneal or oral administration. *Toxicology*, *284*(1–3), 1–6. https://doi.org/10.1016/j.tox.2011.02.005

Dechraoui, M.-Y., Naar, J., Pauillac, S., & Legrand, A.-M. (1999). Ciguatoxins and brevetoxins, neurotoxic polyether compounds active on sodium channels. *Toxicon*, *37*(1), 125–143. https://doi.org/10.1016/s0041-0101(98)00169-x

Dickey, R. W., & Plakas, S. M. (2010). Ciguatera: A public health perspective. *Toxicon*, *56*(2), 123–136. https://doi.org/10.1016/j.toxicon.2009.09.008

Edmunds, J. S. G., McCarthy, R. A., & Ramsdell, J. S. (1999). Ciguatoxin reduces larval survivability in finfish. *Toxicon*, *37*(12), 1827–1832. https://doi.org/10.1016/s0041-0101(99)00119-1

Estevez, P., Castro, D., Manuel Leao, J., Yasumoto, T., Dickey, R., & Gago-Martinez, A. (2019). Implementation of liquid chromatography tandem mass spectrometry for the analysis of Ciguatera fish poisoning in contaminated fish samples from Atlantic coasts. *Food Chemistry*, *280*, 8–14. https://doi.org/10.1016/j.foodchem.2018.12.038

Estevez, P., Sibat, M., Leão-Martins, J. M., Reis Costa, P., Gago-Martínez, A., & Hess, P. (2020). Liquid chromatography coupled to high-resolution mass spectrometry for the confirmation of Caribbean ciguatoxin-1 as the main toxin responsible for ciguatera poisoning caused by fish from European Atlantic coasts. *Toxins*, *12*(4), 267. https://doi.org/10.3390/toxins12040267

Fekete, S. (2021). Defining material used in biopharmaceutical analysis. *LCGC Europe*, 245–248. https://doi.org/10.56530/lcgc.eu.bq1982p9

Fleming, L. E., & Blythe, D. (1997). Ciguatera Fish Poisoning. *Shoreman's Travel Med.*

Mon. 1, 1–5.

Friedman, M., Fernandez, M., Backer, L., Dickey, R., et.al. (2017). An updated review of Ciguatera fish poisoning: Clinical, epidemiological, environmental, and Public Health Management. *Marine Drugs*, *15*(3), 72. https://doi.org/10.3390/md15030072

Friedman, M., Fleming, L., Fernandez, M., Bienfang, P., et. al. (2008). Ciguatera fish poisoning: Treatment, prevention and management. *Marine Drugs*, *6*(3), 456–479. https://doi.org/10.3390/md6030456

Gatti, C., Oelher, E., & Legrand, A. M. (2008). Severe seafood poisoning in French Polynesia: A retrospective analysis of 129 medical files. *Toxicon*, *51*(5), 746–753. https://doi.org/10.1016/j.toxicon.2007.11.025

Gatti, Clémence, Lonati, D., Darius, H., Zancan, A., Roué, M., Schicchi, A., Locatelli, C., & Chinain, M. (2018). *Tectus niloticus* (Tegulidae, gastropod) as a novel vector of Ciguatera poisoning: Clinical characterization and follow-up of a mass poisoning event in Nuku Hiva Island (French Polynesia). *Toxins*, *10*(3), 102. https://doi.org/10.3390/toxins10030102

Gosetti, F., Mazzucco, E., Zampieri, D., & Gennaro, M. C. (2010). Signal Suppression/enhancement in high-performance liquid chromatography tandem mass spectrometry. *Journal of Chromatography A*, *1217*(25), 3929–3937. https://doi.org/10.1016/j.chroma.2009.11.060

Gross, J. H. (2011). Mass Spectrometry. *Springer Heidelberg.* https://doi.org/10.1007/978-3-642-10711-5

Gross, M. L. (1994). Accurate masses for structure confirmation. *Journal of the American Society for Mass Spectrometry*, *5*(2), 57–57. https://doi.org/10.1016/1044- 0305(94)85036-4

Gwinn, J. K., Uhlig, S., Ivanova, L., Fæste, C. K., Kryuchkov, F., & Robertson, A. (2021). In vitro glucuronidation of Caribbean ciguatoxins in fish: First report of conjugative ciguatoxin metabolites. *Chemical Research in Toxicology*, *34*(8), 1910–1925. https://doi.org/10.1021/acs.chemrestox.1c00181

Hamilton, B., Hurbungs, M., Jones, A., & Lewis, R. J. (2002). Multiple ciguatoxins present in Indian Ocean Reef Fish. *Toxicon*, *40*(9), 1347–1353. https://doi.org/10.1016/s0041-0101(02)00146-0

Harwood, D. T., Murray, S., & Boundy, M. J. (2017). Sample preparation prior to marine toxin analysis. *Recent Advances in the Analysis of Marine Toxins*, *78*, 89–136. https://doi.org/10.1016/bs.coac.2017.07.003

Hopfgartner, G. (2017). Wilfried M. A. Niessen and Ricardo A. Correra C.: Interpretation of MS-MS mass spectra of drugs and pesticides. *Analytical and Bioanalytical Chemistry*, *409*(30), 6935–6936. https://doi.org/10.1007/s00216-017-0694-y

Ingle, J. D. (1974). Sensitivity and limit of detection in quantitative spectrometric methods. *Journal of Chemical Education*, *51*(2), 100. https://doi.org/10.1021/ed051p100

Jakob, A., Grilc, M., Teržan, J., & Likozar, B. (2021). Solubility temperature dependence of bio-based Levulinic acid, furfural, and hydroxymethylfurfural in water, nonpolar, polar aprotic and protic solvents. *Processes*, *9*(6), 924. https://doi.org/10.3390/pr9060924

Jauffrais, T., Marcaillou, C., Herrenknecht, C., Truquet, P., Séchet, V., Nicolau, E., Tillmann, U., & Hess, P. (2012). Azaspiracid accumulation, detoxification and biotransformation in blue mussels (*Mytilus edulis*) experimentally fed azadinium spinosum. *Toxicon*, *60*(4), 582–595. https://doi.org/10.1016/j.toxicon.2012.04.351

Jiang, X.-W., Li, X., Lam, P. K., Cheng, S. H., Schlenk, D., Mitcheson, Y. S., Li, Y., Gu, J.-D., & Chan, L. L. (2012). Proteomic analysis of hepatic tissue of ciguatoxin (CTX) contaminated coral reef fish *Cephalopholis argus* and moray eel *Gymnothorax undulatus*. *Harmful Algae*, *13*, 65–71. https://doi.org/10.1016/j.hal.2011.10.009

Kebarle, P., & Tang, L. (1993). From ions in solution to ions in the gas phase - the mechanism of Electrospray Mass Spectrometry. *Analytical Chemistry*, *65*(22), 972-986. https://doi.org/10.1021/ac00070a001

Kostiainen, R., & Kauppila, T. J. (2009). Effect of eluent on the ionization process in liquid chromatography–mass spectrometry. *Journal of Chromatography A*, *1216*(4), 685–699. https://doi.org/10.1016/j.chroma.2008.08.095

Lange, W. R. (1992). Travel and Ciguatera Fish poisoning. *Archives of Internal Medicine*, *152*(10), 2049. https://doi.org/10.1001/archinte.1992.00400220075013

Lappas, N. T., & Lappas, C. M. (2016). Methods of detection, identification, and Quantitation. *Forensic Toxicology*, 161–181. https://doi.org/10.1016/b978-0-12-799967-8.00010-4

Leite, I. do, Sdiri, K., Taylor, A., Viallon, J., Gharbia, H. B., Mafra Júnior, L. L., Swarzenski, P., Oberhaensli, F., Darius, H. T., Chinain, M., & Bottein, M.-Y. D. (2021). Experimental evidence of ciguatoxin accumulation and depuration in carnivorous lionfish. *Toxins*, *13*(8), 564. https://doi.org/10.3390/toxins13080564

Lewis, R. J. (1992). Ciguatoxins are potent ichthyotoxins. *Toxicon*, *30*(2), 207–211. https://doi.org/10.1016/0041-0101(92)90474-j

Lewis, R. J. (2001). The changing face of ciguatera. *Toxicon*, *39*(1), 97–106. https://doi.org/10.1016/s0041-0101(00)00161-6

Lewis, R. J., & Holmes, M. J. (1993). Origin and transfer of toxins involved in Ciguatera. *Comparative Biochemistry and Physiology Part C: Pharmacology, Toxicology and Endocrinology*, *106*(3), 615–628. https://doi.org/10.1016/0742-8413(93)90217-9

Lewis, R. J., & Sellin, M. (1992). Multiple ciguatoxins in the flesh of fish. *Toxicon*, *30*(8), 915–919. https://doi.org/10.1016/0041-0101(92)90390-q

Lewis, R. J., Jones, A., & Vernoux, J.-P. (1998a). HPLC/tandem electrospray mass spectrometry for the determination of sub-ppb levels of Pacific and Caribbean ciguatoxins in crude extracts of fish. *Analytical Chemistry*, *71*(1), 247–250. https://doi.org/10.1021/ac980598h

Lewis, R. J., Jones, A., & Vernoux, J.-P. (1998b). HPLC/tandem electrospray mass spectrometry for the determination of sub-ppb levels of Pacific and Caribbean ciguatoxins in crude extracts of fish. *Analytical Chemistry*, *71*(1), 247–250. https://doi.org/10.1021/ac980598h

Lewis, R. J., Sellin, M., Poli, M. A., Norton, R. S., MacLeod, J. K., & Sheil, M. M. (1991). Purification and characterization of ciguatoxins from moray eel

(*Lycodontis Javanicus*, Muraenidae). *Toxicon*, *29*(9), 1115–1127. https://doi.org/10.1016/0041-0101(91)90209-a

Lewis, R. J., Yang, A., & Jones, A. (2009a). Erratum to ‘“rapid extraction combined with LC-tandem mass spectrometry (CREM-LC/MS/MS) for the determination of ciguatoxins in Ciguateric Fish flesh”. *Toxicon*, *54*(6), 897. https://doi.org/10.1016/j.toxicon.2009.06.025

Lewis, R. J., Yang, A., & Jones, A. (2009b). Rapid extraction combined with LC-tandem mass spectrometry (CREM-LC/ms/ms) for the determination of ciguatoxins in Ciguateric Fish flesh. *Toxicon*, *54*(1), 62–66. https://doi.org/10.1016/j.toxicon.2009.03.013

Li, C., Chu, S., Tan, S., Yin, X., Jiang, Y., Dai, X., Gong, X., Fang, X., & Tian, D. (2021). Towards higher sensitivity of mass spectrometry: A perspective from the mass analyzers. *Frontiers in Chemistry*, *9*, 1-21. https://doi.org/10.3389/fchem.2021.813359

Li, J., Mak, Y. L., Chang, Y.-H., Xiao, C., Chen, Y.-M., Shen, J., Wang, Q., Ruan, Y., & Lam, P. K. (2020). Uptake and depuration kinetics of Pacific ciguatoxins in orange-spotted grouper (*Epinephelus coioides*). *Environmental Science & Technology*, *54*(7), 4475–4483. https://doi.org/10.1021/acs.est.9b07888

Lopes, V. M., Baptista, M., Repolho, T., Rosa, R., & Costa, P. R. (2014). Uptake, transfer and elimination kinetics of paralytic shellfish toxins in common octopus (*Octopus vulgaris*). *Aquatic Toxicology*, *146*, 205–211. https://doi.org/10.1016/j.aquatox.2013.11.011

MacLean, B., Tomazela, D. M., Abbatiello, S. E., Zhang, S., Whiteaker, J. R., Paulovich, A. G., Carr, S. A., & MacCoss, M. J. (2010). Effect of collision energy optimization on the measurement of peptides by selected reaction monitoring (SRM) mass spectrometry. *Analytical Chemistry*, *82*(24), 10116–10124. https://doi.org/10.1021/ac102179j

Mak, Y. L., Li, J., Liu, C.-N., Cheng, S. H., Lam, P. K. S., Cheng, J., & Chan, L. L. (2017). Physiological and behavioural impacts of Pacific ciguatoxin-1 (P-CTX-1) on Marine Medaka (*Oryzias melastigma*). *Journal of Hazardous Materials*, *321*, 782–790. https://doi.org/10.1016/j.jhazmat.2016.09.066

Mak, Y. L., Wai, T.-C., Murphy, M. B., Chan, W. H., Wu, J. J., Lam, J. C., Chan, L. L., & Lam, P. K. (2013). Pacific ciguatoxins in food web components of coral reef systems in the Republic of Kiribati. *Environmental Science & Technology*, *47*(24), 14070–14079. https://doi.org/10.1021/es403175d

Mattei, C., Molgó, J., & Benoit, E. (2014). Involvement of both sodium influx and potassium efflux in ciguatoxin-induced nodal swelling of frog myelinated axons. *Neuropharmacology*, *85*, 417–426. https://doi.org/10.1016/j.neuropharm.2014.06.00

Matuszewski, B. K., Constanzer, M. L., & Chavez-Eng, C. M. (1998). Matrix effect in quantitative LC/MS/MS analyses of biological fluids: a method for determination of finasteride in human plasma at picogram per milliliter concentrations. *Analytical Chemistry*, *70*(5), 882–889. https://doi.org/10.1021/ac971078+

Matuszewski, B. K., Constanzer, M. L., & Chavez-Eng, C. M. (2003). Strategies for the assessment of matrix effect in quantitative bioanalytical methods based on HPLC−MS/MS. *Analytical Chemistry*, *75*(13), 3019–3030. https://doi.org/10.1021/ac020361s

Moestrup, Ø. (2015). Marine benthic dinoflagellates—unveiling their worldwide biodiversity. *Phycologia*, *54*(1), 87–88. https://doi.org/10.2216/5401br01

Mudge, E. M., Miles, C. O., Ivanova, L., Uhlig, S., James, K. S., Erdner, D. L., Fæste, C. K., McCarron, P., & Robertson, A. (2023). Algal ciguatoxin identified as source of Ciguatera poisoning in the Caribbean. *Chemosphere*, *330*, 138659. https://doi.org/10.1016/j.chemosphere.2023.138659

Munschy, C., Héas-Moisan, K., Tixier, C., Olivier, N., Gastineau, O., Le Bayon, N., & Buchet, V. (2011). Dietary exposure of juvenile common sole (S*olea solea L.*) to polybrominated diphenyl ethers (PBDES): Part 1. bioaccumulation and elimination kinetics of individual congeners and their debrominated metabolites. *Environmental Pollution*, *159*(1), 229–237. https://doi.org/10.1016/j.envpol.2010.09.00

Murata, M., Legrand, A. M., Ishibashi, Y., & Yasumoto, T. (1989). Structures of ciguatoxin and its Congener. *Journal of the American Chemical Society*, *111*(24), 8929–8931. https://doi.org/10.1021/ja00206a032

Murata, M., Legrand, A. M., Ishibashi, Y., Fukui, M., & Yasumoto, T. (1990). Structures and configurations of ciguatoxin from the moray eel *Gymnothorax javanicus* and its likely precursor from the Dinoflagellate *Gambierdiscus toxicus*. *Journal of the American Chemical Society*, *112*(11), 4380–4386. https://doi.org/10.1021/ja00167a040

Murray, J. S., Boundy, M. J., Selwood, A. I., & Harwood, D. T. (2018). Development of an LC–MS/MS method to simultaneously monitor maitotoxins and selected ciguatoxins in algal cultures and P-CTX-1B in Fish. *Harmful Algae*, *80*, 80–87. https://doi.org/10.1016/j.hal.2018.09.00

Nicholson, G., & Lewis, R. (2006). Ciguatoxins: Cyclic polyether modulators of voltage-gated ion channel function. *Marine Drugs*, *4*(3), 82–118. https://doi.org/10.3390/md403082

Nielsen, L. T., Hansen, P. J., Krock, B., & Vismann, B. (2016). Accumulation, transformation and breakdown of DSP toxins from the toxic dinoflagellate *Dinophysis acuta* in blue mussels, *Mytilus edulis*. *Toxicon*, *117*, 84–93. https://doi.org/10.1016/j.toxicon.2016.03.02

Nijat, D., Abdulla, R., Liu, G., Luo, Y., & Aisa, H. A. (2020). Identification and quantification of Meiguihua oral solution using liquid chromatography combined with hybrid quadrupole-orbitrap and triple quadrupole mass spectrometers. *Journal of Chromatography B*, *1139*, 121992. https://doi.org/10.1016/j.jchromb.2020.121992

Page, J. S., Kelly, R. T., Tang, K., & Smith, R. D. (2007a). Ionization and transmission efficiency in an electrospray ionization—mass spectrometry interface. *Journal of the American Society for Mass Spectrometry*, *18*(9), 1582–1590. https://doi.org/10.1016/j.jasms.2007.05.018

Page, J. S., Kelly, R. T., Tang, K., & Smith, R. D. (2007b). Ionization and transmission efficiency in an electrospray ionization—mass spectrometry interface. *Journal of the American Society for Mass Spectrometry*, *18*(9), 1582–1590. https://doi.org/10.1016/j.jasms.2007.05.018

Pasinszki, T., Lako, J., & Dennis, T. E. (2020). Advances in detecting ciguatoxins in fish.*Toxins*, *12*(8), 494. https://doi.org/10.3390/toxins12080494

Pottier, I., Lewis, R. J., & Vernoux, J.-P. (2023). Ciguatera fish poisoning in the Caribbean Sea and Atlantic Ocean: Reconciling the multiplicity of ciguatoxins and analytical chemistry approach for public health safety. *Toxins*, *15*(7), 453. https://doi.org/10.3390/toxins15070453

Prabhu, G. R., Ponnusamy, V. K., Witek, H. A., & Urban, P. L. (2020). Sample flow rate scan in electrospray ionization mass spectrometry reveals alterations in protein charge state distribution. *Analytical Chemistry*, *92*(19), 13042–13049. https://doi.org/10.1021/acs.analchem.0c01945

Ramos-Sosa, M. J., García-Álvarez, N., Sanchez-Henao, A., Silva Sergent, F., Padilla, D., Estévez, P., Caballero, M. J., Martín-Barrasa, J. L., Gago-Martínez, A., Diogène, J., & Real, F. (2022). Ciguatoxin detection in flesh and liver of relevant fish species from the Canary Islands. *Toxins*, *14*(1), 46. https://doi.org/10.3390/toxins14010046

Rockwood, A. L., Kushnir, M. M., & Clarke, N. J. (2018). Mass spectrometry. *Principles and Applications of Clinical Mass Spectrometry*, *2*, 33–65. https://doi.org/10.1016/b978-0-12-816063-3.00002-5

Rousseaux, C. G., Haschek, W. M., & Wallig, M. A. (2013). Safety assessment in toxicologic pathology: An introduction. *Haschek and Rousseaux's Handbook of Toxicologic Pathology, 2*, 643–644. https://doi.org/10.1016/b978-0-12-415759-0.00095-9

Roué, M., Darius, H., Ung, A., Viallon, J., Sibat, M., Hess, P., Amzil, Z., & Chinain, M. (2018). Tissue distribution and elimination of ciguatoxins in *Tridacna maxima* (Tridacnidae, Bivalvia) fed gambierdiscus polynesiensis. *Toxins*, *10*(5), 189. https://doi.org/10.3390/toxins10050189

Révész, Á., Rokob, T. A., Jeanne Dit Fouque, D., Turiák, L., Memboeuf, A., Vékey, K., & Drahos, L. (2018). Selection of collision energies in proteomics mass spectrometry experiments for best peptide identification: Study of mascot score energy dependence reveals double optimum. *Journal of Proteome Research*, *17*(5), 1898–1906. https://doi.org/10.1021/acs.jproteome.7b00912

Sanchez-Henao, J. A., García-Álvarez, N., Fernández, A., Saavedra, P., Silva Sergent, F., Padilla, D., Acosta-Hernández, B., Martel Suárez, M., Diogène, J., & Real, F. (2019). Predictive score and probability of CTX-like toxicity in fish samples from

the official control of Ciguatera in the Canary Islands. *Science of The Total Environment*, *673*, 576–584. https://doi.org/10.1016/j.scitotenv.2019.03.445

Satake, M., Morohashi, A., Oguri, H., Oishi, T., Hirama, M., Harada, N., & Yasumoto, T. (1997). The absolute configuration of ciguatoxin. *Journal of the American Chemical Society*, *119*(46), 11325–11326. https://doi.org/10.1021/ja972482t

Scheuer, P. J., Takahashi, W., Tsutsumi, J., & Yoshida, T. (1967). Ciguatoxin: Isolation and Chemical Nature. *Science*, *155*(3767), 1267–1268. https://doi.org/10.1126/science.155.3767.1267

Sibat, M., Herrenknecht, C., Darius, H. T., Roué, M., Chinain, M., & Hess, P. (2018). Detection of pacific ciguatoxins using liquid chromatography coupled to either low or high resolution mass spectrometry (LC-MS/MS). *Journal of Chromatography A*, *1571*, 16–28. https://doi.org/10.1016/j.chroma.2018.08.008

Soliño, L., & Costa, P. R. (2018). Differential toxin profiles of ciguatoxins in marine organisms: Chemistry, fate and global distribution. *Toxicon*, *150*, 124–143. https://doi.org/10.1016/j.toxicon.2018.05.005

Soliño, L., & Costa, P. R. (2020). Global impact of ciguatoxins and ciguatera fish poisoning on fish, fisheries and consumers. *Environmental Research*, *182*, 109111. https://doi.org/10.1016/j.envres.2020.109111

Sparrow, L., & Heimann, K. (2016). Key environmental factors in the management of Ciguatera. *Journal of Coastal Research*, *75*(sp1), 1007–1011. https://doi.org/10.2112/si75-202.1

Spielmeyer, A., Loeffler, C. R., & Kappenstein, O. (2022). Identical ciguatoxin-3c group profiles in *Lutjanus bohar* from the Pacific and Indian Oceans - indicating the need to re-evaluate geographical CTX classifications. *Frontiers in Marine Science*, *9*, 1-15. https://doi.org/10.3389/fmars.2022.937438

Spielmeyer, A., Loeffler, C., & Bodi, D. (2021). Extraction and LC-MS/MS analysis of Ciguatoxins: A semi-targeted approach designed for fish of unknown origin. *Toxins*, *13*(9), 630. https://doi.org/10.3390/toxins13090630

Stewart, I., Eaglesham, G. K., Poole, S., Graham, G., Paulo, C., Wickramasinghe, W., Sadler, R., & Shaw, G. R. (2010). Establishing a public health analytical service

based on chemical methods for detecting and quantifying pacific ciguatoxin in fish samples. *Toxicon*, *56*(5), 804–812. https://doi.org/10.1016/j.toxicon.2009.07.028

Tester, P. A., Litaker, R. W., & Berdalet, E. (2020). Climate change and harmful benthic microalgae. *Harmful Algae*, *91*, 101655. https://doi.org/10.1016/j.hal.2019.101655

Van Eeckhaut, A., Lanckmans, K., Sarre, S., Smolders, I., & Michotte, Y. (2009). Validation of bioanalytical LC–MS/MS assays: Evaluation of matrix effects. *Journal of Chromatography B*, *877*(23), 2198–2207. https://doi.org/10.1016/j.jchromb.2009.01.003

Vernoux, J.-P., & Lewis, R. J. (1997). Isolation and characterisation of Caribbean ciguatoxins from the horse-eye jack (*Caranx latus*). *Toxicon*, *35*(6), 889–900. https://doi.org/10.1016/s0041-0101(96)00191-2

Wang, D.-Z. (2008). Neurotoxins from marine dinoflagellates: A brief review. *Marine Drugs*, *6*(2), 349–371. https://doi.org/10.3390/md20080016

Wang, P. G., & Zhou, W. (2016). Rapid determination of cocamidopropyl betaine impurities in cosmetic products by core-shell hydrophilic interaction liquid chromatography-tandem mass spectrometry. *Journal of Chromatography A*, *1461*, 78–83. https://doi.org/10.1016/j.chroma.2016.07.056

WHO, F. (2018). Report of the expert meeting on Ciguatera poisoning. *World Health Organization*. Geneva, Switzerland. https://doi.org/10.4060/ca8817en

World Health Organization. (2023). *Chemical safety*. World Health Organization. https://www.who.int/health-topics/chemical-safety

Wu, J. J., Mak, Y. L., Murphy, M. B., Lam, J. C., Chan, W. H., Wang, M., Chan, L. L., & Lam, P. K. (2011). Validation of an accelerated solvent extraction liquid chromatography–tandem mass spectrometry method for pacific ciguatoxin-1 in fish flesh and comparison with the Mouse Neuroblastoma Assay. *Analytical and Bioanalytical Chemistry*, *400*(9), 3165–3175. https://doi.org/10.1007/s00216-011-4977-4

Yan, M., Leung, P. T. Y., Ip, J. C. H., Cheng, J., Wu, J.-J., Gu, J.-R., & Lam, P. K. S.

(2017). Developmental toxicity and molecular responses of Marine Medaka (*Oryzias melastigma*) embryos to ciguatoxin P-CTX-1 exposure. *Aquatic Toxicology*, *185*, 149–159. https://doi.org/10.1016/j.aquatox.2017.02.006

Yan, M., Mak, M. Y. L., Cheng, J., Li, J., Gu, J. R., Leung, P. T. Y., & Lam, P. K. S. (2020). Effects of dietary exposure to ciguatoxin P-CTX-1 on the reproductive performance in Marine Medaka (*Oryzias melastigma*). *Marine Pollution Bulletin*, *152*, 110837. https://doi.org/10.1016/j.marpolbul.2019.110837

Yogi, K., Oshiro, N., Inafuku, Y., Hirama, M., & Yasumoto, T. (2011). Detailed LC-MS/MS analysis of ciguatoxins revealing distinct regional and species characteristics in fish and causative alga from the Pacific. *Analytical Chemistry*, *83*(23), 8886–8891. https://doi.org/10.1021/ac200799j

Yon, T., Sibat, M., Réveillon, D., Bertrand, S., Chinain, M., & Hess, P. (2021). Deeper insight into *Gambierdiscus polynesiensis* toxin production relies on specific optimization of high-performance liquid chromatography-high resolution mass spectrometry. *Talanta*, *232*, 122400. https://doi.org/10.1016/j.talanta.2021.122400

Appendix

Table A1: Peak intensities at flow rates 1, 5, and 10 uL/min.

Flow Rate (uL/min)	Peak Intensity		
	$[M+H]^+$	$[M+NH_4]^+$	$[M+Na]^+$
1	4.11E+04	5.75E+04	6.56E+04
1	1.33E+04	1.44E+04	7.62E+03
1	1.57E+04	1.48E+04	9.49E+03
1	1.42E+04	1.33E+04	1.03E+04
1	2.44E+04	3.36E+04	1.77E+04
1	2.21E+03	5.91E+03	1.67E+03
5	1.59E+04	2.10E+04	1.19E+04
5	1.76E+04	2.39E+04	1.43E+04
5	2.27E+04	2.56E+04	1.50E+04
5	1.16E+04	1.51E+04	7.75E+03
10	3.36E+04	4.07E+04	2.31E+04
10	4.87E+04	5.98E+04	3.25E+04
10	4.71E+04	5.28E+04	3.05E+04

Table A2: Matrix Effect Factor: Neat standard

Ion	Mass accuracy (ppm)	Peak height
$[M+H-H_20]^+$	15.3	1.85E+04
	12.2	1.16E+04
$[M+H]^+$	1.6	8.07E+04
	1.0	8.07E+04
	3.6	2.05E+04
	2.6	4.44E+04
	7.1	3.62E+02
$[M+NH_4]^+$	-4.6	5.43E+04
	-6.6	3.47E+04
	-2.1	1.16E+04
	-1.5	1.89E+03
	3.3	1.16E+03
$[M+Na]^+$	9.2	5.86E+03
	17.6	2.18E+03

Table A3: Matrix Effect Factor: Sample

Ion	Mass accuracy (ppm)	Peak height
$[M+H-H_20]^+$	54.2	3.96E+05
	58	2.69E+05
$[M+H]^+$	77.9	8.41E+05
	80.7	5.09E+05
	94.6	1.39E+06
	68.1	1.39E+06
	2.9	4.65E+05
$[M+NH_4]^+$	89.9	3.81E+05
	96.9	1.11E+06
	102.8	6.41E+05
	111.8	1.39E+06
	88.7	4.34E+05
$[M+Na]^+$	69.7	1.02E+06
	71.9	1.39E+06

Table A4: Matrix Effect Factor for the most intense ions.

Ion	MEF
$[M+H-H_20]^+$	21.41
$[M+H]^+$	10.42
$[M+NH_4]^+$	7.02
$[M+Na]^+$	174.06

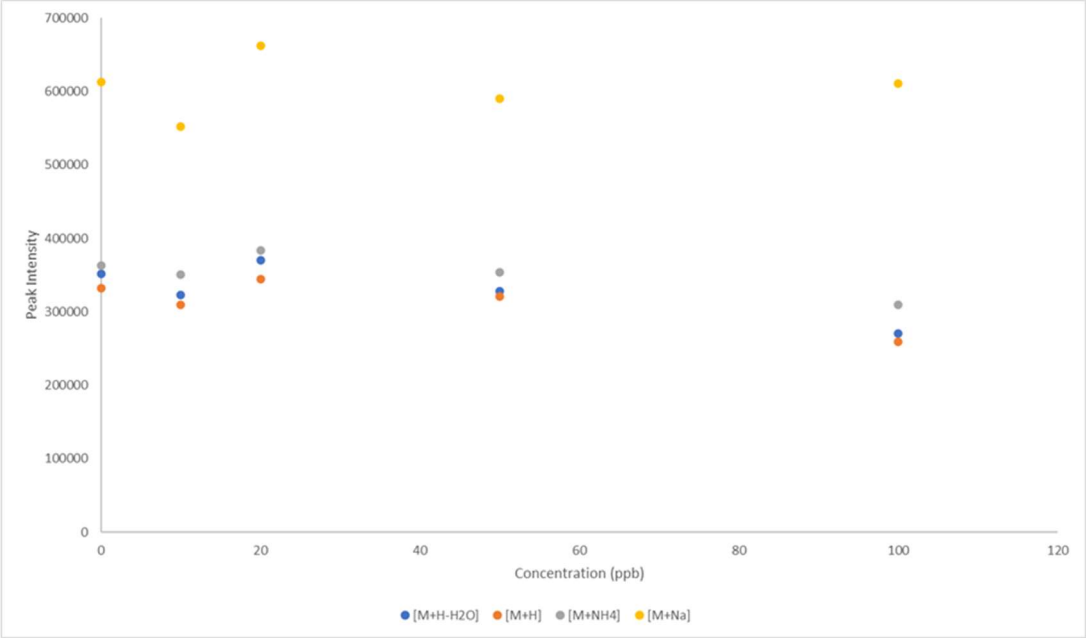

Figure A1: Concentration of fish sample spiked with 10, 20, 50, and 100 ppb of P-CTX3C standard after sample preparation and SPE versus peak intensity. Calibrations solutions 1 (prepared on the on the same day as the spiked fish sample) Blue: $[M+H-H_2O]^+$ Orange: $[M+H]^+$ Grey: $[M+NH_4]^+$ Yellow: $[M+Na]^+$

Table A5: Concentration of fish sample spiked with 10, 20, 50, and 100 ppb of P-CTX3C standard after sample preparation and SPE versus peak intensity. Prepared on the on the same day as the toxic fish sample.

Concentration of PCTX-3B (ppb)	Peak Intensity			
	[M+H-H_2O]	[M+H]	[M+NH_4]	[M+Na]
0	3.52E+05	3.32E+05	3.63E+05	6.13E+05
10	3.23E+05	3.10E+05	3.51E+05	5.52E+05
20	3.71E+05	3.44E+05	3.83E+05	6.62E+05
50	3.28E+05	3.21E+05	3.54E+05	5.90E+05
100	2.71E+05	2.59E+05	3.10E+05	6.11E+05

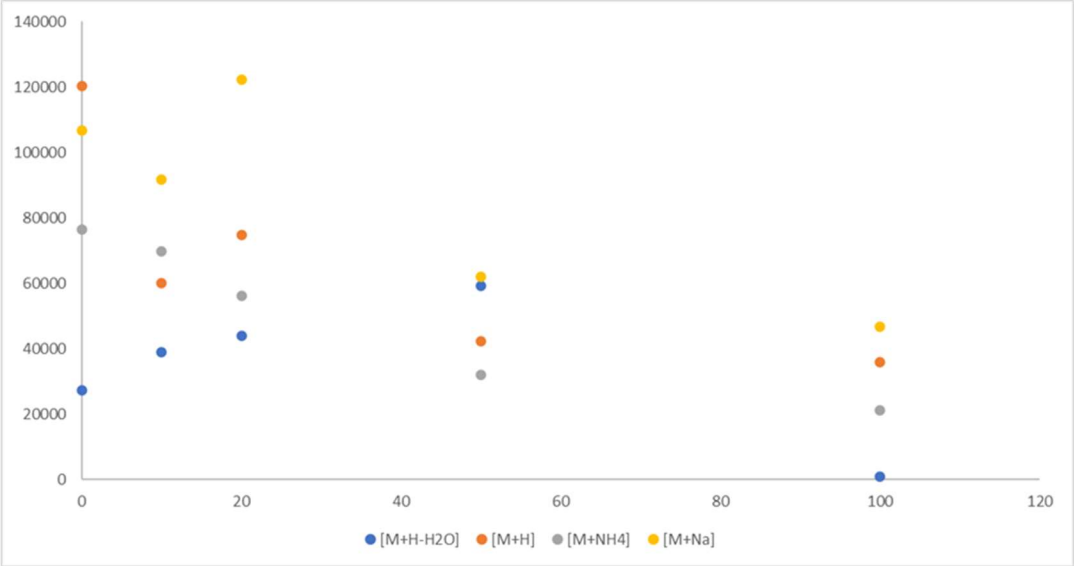

Figure A2: Concentration of fish sample spiked with 10, 20, 50, and 100 ppb of P-CTX3C standard after sample preparation and SPE versus peak intensity. Calibration solution 2 (prepared on a separate day from the spiked fish sample). Blue: $[M+H-H_2O]^+$ Orange: $[M+H]^+$ Grey: $[M+NH_4]^+$ Yellow: $[M+Na]^+$

Table A6: Concentration of fish sample spiked with 10, 20, 50, and 100 ppb of P-CTX3C standard after sample preparation and SPE versus peak intensity. Prepared on a separate day from the toxic fish sample. Blue: $[M+H-H_2O]^+$ Orange: $[M+H]^+$ Grey: $[M+NH_4]^+$ Yellow: $[M+Na]^+$

Concentration of PCTX-3B (ppb)	Peak Intensity			
	$[M+H-H_2O]$	$[M+H]$	$[M+NH_4]$	$[M+Na]$
0	2.73E+04	1.20E+05	7.64E+04	1.07E+05
10	3.90E+04	6.02E+04	6.99E+04	9.19E+04
20	4.40E+04	7.47E+04	5.62E+04	1.22E+05
50	5.93E+04	4.24E+04	3.19E+04	6.19E+04
100	8.18E+02	3.58E+04	2.11E+04	4.66E+04

Table A7: F statistic value and p value for calibration curve.

50.49343832	F statistic	k	1
0.980765008	p value	n	4
		R squared	0.9619

pvalue > 0.05